

Nonadiabatic Field on Quantum Phase Space: A Century after Ehrenfest

Baihua Wu, Xin He, and Jian Liu*



Cite This: *J. Phys. Chem. Lett.* 2024, 15, 644–658



Read Online

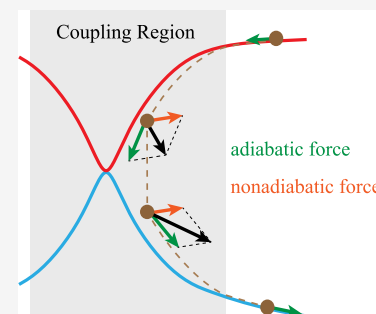
ACCESS |

Metrics & More

Article Recommendations

Supporting Information

ABSTRACT: Nonadiabatic transition dynamics lies at the core of many electron/hole transfer, photoactivated, and vacuum field-coupled processes. About a century after Ehrenfest proposed “*Phasenraum*” and the Ehrenfest theorem, we report a conceptually novel trajectory-based nonadiabatic dynamics approach, nonadiabatic field (NAF), based on a generalized exact coordinate–momentum phase space formulation of quantum mechanics. It does not employ the conventional Born–Oppenheimer or Ehrenfest trajectory in the nonadiabatic coupling region. Instead, in NAF the equations of motion of the independent trajectory involve a nonadiabatic nuclear force term in addition to an adiabatic nuclear force term of a single electronic state. A few benchmark tests for gas phase and condensed phase systems indicate that NAF offers a practical tool to capture the correct correlation of electronic and nuclear dynamics for processes where the states remain coupled all the time as well as for the asymptotic region where the coupling of electronic states vanishes.



Since Paul Ehrenfest and Tatyana Ehrenfest first used “*Phasenraum*” in 1911, the expression “phase space” has been widely employed.^{1,2} In classical mechanics, phase space with coordinate–momentum variables presents a fundamental concept and tool.^{3,4} Phase space formulations with coordinate–momentum variables also offer an exact interpretation of quantum mechanics for continuous-variable systems,^{5–9} for which pioneering works were demonstrated by Weyl and Wigner^{5,6} and a unified scheme was later presented by Cohen.¹⁰ More recently, we have proposed a generalized exact coordinate–momentum phase space formulation of quantum mechanics for composite systems, where both continuous and discrete variables are involved.^{11–18} It maps discrete degrees of freedom (DOFs) onto the *constraint* coordinate–momentum *phase space* (CPS) and continuous DOFs onto the infinite coordinate–momentum phase space. Trajectory-based dynamics is derived from the symplectic structure of mapping phase space where the generated mapping Hamiltonian is conserved. The generalized exact coordinate–momentum phase space formulation then offers a framework to develop approximate but practically useful dynamics approaches for studying composite systems^{16,17} that include coupled multi-electronic-state systems that appear in such areas as photochemistry, charge (electron/hole) and electronic energy transfer, cavity modified phenomena, etc.^{19–29} Such important processes involve the quantum mechanical behavior of both electrons and nuclei in the context of nonadiabatic dynamics, where electronic DOFs are often described by the discrete (adiabatic or diabatic) state representation and nuclear DOFs are depicted in continuous space.

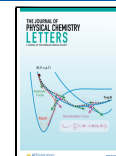
Paul Ehrenfest also proposed the Ehrenfest theorem³⁰ in 1927. It has led to a simple and convenient mean field approach, also called Ehrenfest dynamics. Early examples of application of the Ehrenfest theorem to chemical dynamics include refs 105–108. Although it is not clear to us when the Ehrenfest theorem was first used to study electronically nonadiabatic transition processes, Ehrenfest dynamics has been a conventional practical approach in the field of nonadiabatic dynamics. (Please see more discussion in Section S8 of the Supporting Information.) It involves the independent trajectory, for which the evolution of nuclei is governed by the mean field force that is independent of the representation of the electronic basis sets. Ehrenfest dynamics is useful for describing the dynamical behavior in the coupling region but fails to capture the bifurcation characteristic for the nuclear motion in the asymptotic region, where the coupling of electronic states vanishes. Another prevailing category of trajectory-based nonadiabatic methods employs the independent Born–Oppenheimer trajectory, of which the nuclear force is produced from a single adiabatic potential energy surface (PES). For example, surface hopping (SH) methods^{31–37} (pioneered by Tully^{38,39}) have been developed by using various hopping mechanisms to connect two independent Born–Oppenheimer trajectories on two different adiabatic

Received: December 2, 2023

Revised: December 22, 2023

Accepted: January 3, 2024

Published: January 11, 2024



PESs in the coupling region. Such methods are capable of depicting the correct physical picture for the nuclear motion in the asymptotic region but are often less efficient and/or less accurate in the coupling region. It is often challenging for Born–Oppenheimer trajectory-based methods to describe dynamical processes where the states remain coupled all of the time, especially in the low-temperature regime.

As described in ref 17, three key elements for a trajectory-based quantum dynamics method are the equations of motion (EOMs) of the trajectory, the initial condition of the trajectory, and the integral expression for evaluation of the time-dependent physical property. The generalized exact coordinate–momentum phase space formulation of quantum mechanics provides a new stage for investigating such key elements. In this Perspective, we focus on the investigation of the EOMs in the electronically adiabatic representation based on our previous work in refs 15 and 17. We propose a conceptually novel trajectory-based approach, nonadiabatic field (NAF), by maintaining the nonadiabatic term of the Ehrenfest-like force in addition to a single-state adiabatic nuclear force in the EOMs for nuclear mapping variables. The purpose of this Perspective is to show that NAF is capable of capturing important features in both coupling and asymptotic regions for nonadiabatic molecular dynamics.

Generalized Coordinate–Momentum Phase Space Formulation of Quantum Mechanics.

Consider the full Hamiltonian of nuclei and electrons of the molecular system

$$\hat{H} = \frac{1}{2}\hat{\mathbf{P}}^T \mathbf{M}^{-1} \hat{\mathbf{P}} + \hat{H}_{el}(\hat{\mathbf{R}}) \quad (1)$$

where $\hat{H}_{el}(\hat{\mathbf{R}})$ is the electronic Hamiltonian, $\mathbf{M} = \text{diag}\{m_i\}$ is the diagonal nuclear mass matrix, and $\{\mathbf{R}, \mathbf{P}\}$ are the coordinates and momenta of nuclear degrees of freedom (DOFs). Assume that $\{|n\rangle\}$, $n \in \{1, \dots, F\}$ is the “complete” set of diabatic electronic states and $\{|\phi_k(\mathbf{R})\rangle\}$, $n \in \{1, \dots, F\}$ is the “complete” set of adiabatic electronic states. (F is in general infinite when the set of electronic states is rigorously complete.) The representation of $\hat{H}_{el}(\hat{\mathbf{R}})$ in the diabatic basis reads

$$\hat{H}_{el}(\mathbf{R}) = \sum_{n,m} V_{nm}(\mathbf{R}) |n\rangle \langle m| \equiv \mathbf{V}(\mathbf{R}) \quad (2)$$

and that in the adiabatic basis is

$$\hat{H}_{el}(\mathbf{R}) = \sum_k E_k(\mathbf{R}) |\phi_k(\mathbf{R})\rangle \langle \phi_k(\mathbf{R})| \quad (3)$$

where $E_k(\mathbf{R})$ denotes the adiabatic potential energy surface of the k -th adiabatic electronic state. The expression of eq 3 for the electronic Hamiltonian $\hat{H}_{el}(\mathbf{R})$ in eq 1 first appeared for phase space mapping methods for nonadiabatic dynamics in refs 17 and 40. The generalized coordinate–momentum phase space formulation maps the coupled F -electronic-state Hamiltonian operator (e.g., in the diabatic basis for eqs 1 and 2), $\hat{H} = \sum_{n,m=1}^F \left[\frac{1}{2} \hat{\mathbf{P}}^T \mathbf{M}^{-1} \hat{\mathbf{P}} \delta_{nm} + V_{nm}(\hat{\mathbf{R}}) \right] |n\rangle \langle m|$, to

$$\begin{aligned} H(\mathbf{R}, \mathbf{P}; \mathbf{x}, \mathbf{p}; \Gamma) &= \frac{1}{2} \mathbf{P}^T \mathbf{M}^{-1} \mathbf{P} \\ &+ \sum_{n,m=1}^F \left[\frac{1}{2} (x^{(n)} x^{(m)} + p^{(n)} p^{(m)}) - \Gamma_{nm} \right] V_{mn}(\mathbf{R}) \end{aligned} \quad (4)$$

where $\{\mathbf{x}, \mathbf{p}\} = \{x^{(1)}, \dots, x^{(F)}, p^{(1)}, \dots, p^{(F)}\}$ are the coordinate and momentum variables for representing the discrete

electronic states and Γ is the Hermitian commutator matrix whose elements are variables. For convenience, the potential energy matrix $V_{nm}(\hat{\mathbf{R}})$ is set to be a real symmetric matrix. Commutator matrix Γ was heuristically proposed from the general commutation relation, $[\hat{x}^{(m)}, \hat{p}^{(n)}] + [\hat{x}^{(n)}, \hat{p}^{(m)}] = 2i(\Gamma_{nm} + \Gamma_{mn})$, for the underlying mapping electronic DOFs which are neither bosons nor fermions^{11,15} (with the convention $\hbar = 1$ for electronic DOFs throughout this Perspective). Mapping Hamiltonian eq 4 is rigorously produced from the one-to-one correspondence relation between any quantum operator \hat{A} and its corresponding phase space function

$$A_C(\mathbf{R}, \mathbf{P}; \mathbf{x}, \mathbf{p}; \Gamma) = \text{Tr}_{n,e}[\hat{A} \hat{K}_{\text{nuc}}(\mathbf{R}, \mathbf{P}) \otimes \hat{K}_{\text{ele}}(\mathbf{x}, \mathbf{p}; \Gamma)] \quad (5)$$

Here, $\text{Tr}_n[\cdot]$ and $\text{Tr}_e[\cdot]$ represent the trace over nuclear and electronic DOFs, respectively, and the kernel of the Wigner function⁶ is used as the mapping kernel for continuous (nuclear) DOFs

$$\hat{K}_{\text{nuc}}(\mathbf{R}, \mathbf{P}) = \left(\frac{\hbar}{2\pi} \right)^N \int d\zeta d\eta e^{i\zeta \cdot (\hat{\mathbf{R}} - \mathbf{R}) + i\eta \cdot (\hat{\mathbf{P}} - \mathbf{P})} \quad (6)$$

where N represents the number of dimensions of nuclear DOFs. The mapping relation, eq 5, implies a broad class of mapping kernels on CPS for discrete (electronic) DOFs, e.g.

$$\hat{K}_{\text{ele}}(\mathbf{x}, \mathbf{p}, \Gamma) = \sum_{n,m=1}^F \left[\frac{1}{2} (x^{(n)} + ip^{(n)}) (x^{(m)} - ip^{(m)}) - \Gamma_{nm} \right] |n\rangle \langle m| \quad (7)$$

It is straightforward to show that the mathematical structure of the mapping CPS for eq 7 is related to the quotient space $U(F)/U(F-r)$, namely, the complex Stiefel manifold.^{41–43} Here, $1 \leq r < F$.

Consider the simplest case, $r = 1$. Commutator matrix Γ becomes a constant matrix, i.e., the mapping CPS is reduced to the quotient space $U(F)/U(F-1)$

$$S(\mathbf{x}, \mathbf{p}; \gamma) = \delta \left(\sum_{n=1}^F \frac{(x^{(n)})^2 + (p^{(n)})^2}{2} - (1 + F\gamma) \right) \quad (8)$$

where parameter $\gamma \in (-1/F, \infty)$. The mapping kernel on CPS for discrete (electronic) DOFs, eq 7, is then

$$\hat{K}_{\text{ele}}(\mathbf{x}, \mathbf{p}; \gamma) = \sum_{n,m=1}^F \left[\frac{1}{2} (x^{(n)} + ip^{(n)}) (x^{(m)} - ip^{(m)}) - \gamma \right] |n\rangle \langle m| \quad (9)$$

and mapping Hamiltonian eq 4 then leads to a model reminiscent of the celebrated Meyer–Miller mapping Hamiltonian, which in 1979 Meyer and Miller originally proposed by applying the Langer correction⁴⁴ and in 1997 Stock and Thoss derived by using the Schwinger oscillator model of angular momentum.⁴⁵ The generalized coordinate–momentum phase space formulation suggests that the physical meaning of parameter γ is beyond the conventional zero-point-energy parameter indicated in refs 44 and 45, which takes even negative values and is a special case of the commutator matrix related to the complex Stiefel manifold.^{11,13–17,43} The trace of a product of two quantum operators is expressed as an integral of two functions on mapping coordinate–momentum phase space, that is

$$\text{Tr}_{n,e}[\hat{A}\hat{B}] = \int d\mu_{\text{nuc}}(\mathbf{R}, \mathbf{P}) \int_{S(\mathbf{x}, \mathbf{p}; \gamma)} d\mu_{\text{ele}}(\mathbf{x}, \mathbf{p}; \gamma) A_C(\mathbf{R}, \mathbf{P}; \mathbf{x}, \mathbf{p}; \gamma) \tilde{B}_C(\mathbf{R}, \mathbf{P}; \mathbf{x}, \mathbf{p}; \gamma) \quad (10)$$

with

$$\tilde{B}_C(\mathbf{R}, \mathbf{P}; \mathbf{x}, \mathbf{p}; \gamma) = \text{Tr}_{n,e}[\hat{K}_{\text{nuc}}^{-1}(\mathbf{R}, \mathbf{P}) \otimes \hat{K}_{\text{ele}}^{-1}(\mathbf{x}, \mathbf{p}; \gamma) \hat{B}] \quad (11)$$

$d\mu_{\text{nuc}}(\mathbf{R}, \mathbf{P}) = (2\pi\hbar)^{-N} d\mathbf{R} d\mathbf{P}$ and $d\mu_{\text{ele}}(\mathbf{x}, \mathbf{p}; \gamma) = F d\mathbf{x} d\mathbf{p}$ as the integration measure on infinite phase space for continuous nuclear DOFs and that on CPS for discrete electronic DOFs, respectively. The integral over the mapping CPS variables for electronic DOFs in eq 10 is performed as

$$\int_{S(\mathbf{x}, \mathbf{p})} F d\mathbf{x} d\mathbf{p} g(\mathbf{x}, \mathbf{p}) = \int F d\mathbf{x} d\mathbf{p} \frac{1}{\Omega} S(\mathbf{x}, \mathbf{p}) g(\mathbf{x}, \mathbf{p}) \quad (12)$$

where $\Omega = \int d\mathbf{x} d\mathbf{p} S(\mathbf{x}, \mathbf{p})$ is the area of constraint phase space $S(\mathbf{x}, \mathbf{p})$ as the normalization constant. In eq 11 the inverse mapping kernel for continuous (nuclear) DOFs is

$$\hat{K}_{\text{nuc}}^{-1}(\mathbf{R}, \mathbf{P}) = \left(\frac{\hbar}{2\pi} \right)^N \int d\xi d\eta e^{i\xi \cdot (\hat{\mathbf{R}} - \mathbf{R}) + i\eta \cdot (\hat{\mathbf{P}} - \mathbf{P})} \quad (13)$$

The corresponding inverse mapping kernel for finite discrete electronic DOFs is, however, not unique,^{43,109} even when CPS is the quotient space $U(F)/U(F-1)$. For simplicity, in this Perspective, we use the inverse mapping kernel of refs 13–15

$$\begin{aligned} \hat{K}_{\text{ele}}^{-1}(\mathbf{x}, \mathbf{p}; \gamma) &= \sum_{n,m=1}^F \left[\frac{1+F}{2(1+F\gamma)^2} (x^{(n)} + ip^{(n)}) \right. \\ &\times (x^{(m)} - ip^{(m)}) - \frac{1-\gamma}{1+F\gamma} \delta_{nm} \left. \right] |n\rangle \langle m| \end{aligned} \quad (14)$$

for demonstration. More inverse mapping kernels will be discussed in our forthcoming paper.

Equations of Motion on the Generalized Coordinate–Momentum Phase Space. When operator \hat{B} is replaced by its Heisenberg operator $\hat{B}(t)$, the evaluation of eq 10 is often approximated by trajectory-based dynamics on mapping phase space, e.g.

$$\begin{aligned} \text{Tr}_{n,e}[\hat{A}(0)\hat{B}(t)] &= \int d\mu_{\text{nuc}}(\mathbf{R}, \mathbf{P}) \int_{S(\mathbf{x}, \mathbf{p}; \gamma)} d\mu_{\text{ele}}(\mathbf{x}, \mathbf{p}; \gamma) A_C \\ &(\mathbf{R}, \mathbf{P}; \mathbf{x}, \mathbf{p}; \gamma) \tilde{B}_C(\mathbf{R}, \mathbf{P}; \mathbf{x}, \mathbf{p}; \gamma; t) \approx \int d\mu_{\text{nuc}}(\mathbf{R}, \mathbf{P}) \\ &\int_{S(\mathbf{x}, \mathbf{p}; \gamma)} d\mu_{\text{ele}}(\mathbf{x}, \mathbf{p}; \gamma) A_C(\mathbf{R}, \mathbf{P}; \mathbf{x}, \mathbf{p}; \gamma) \tilde{B}_C(\mathbf{R}, \mathbf{P}; \mathbf{x}, \mathbf{p}; \gamma) \end{aligned} \quad (15)$$

In addition to the integral form of eq 15 for evaluating the time-dependent physical property, the EOMs for the trajectory compatible with the phase space integral expression are another key element.

It is straightforward to follow refs 15 and 17 to show that the symplectic structure of mapping Hamiltonian eq 4 leads to the EOMs in the diabatic representation

$$\dot{\mathbf{x}} + i\dot{\mathbf{p}} = -i\mathbf{V}(\mathbf{R})(\mathbf{x} + i\mathbf{p})$$

$$\dot{\mathbf{R}} = \mathbf{M}^{-1}\mathbf{P}$$

$$\dot{\mathbf{P}} = - \sum_{n,m=1}^F (\nabla_{\mathbf{R}} V_{mn}(\mathbf{R})) \left[\frac{1}{2} (x^{(n)} x^{(m)} + p^{(n)} p^{(m)}) - \Gamma_{nm} \right]$$

$$\dot{\Gamma} = i[\Gamma\mathbf{V}(\mathbf{R}) - \mathbf{V}(\mathbf{R})\Gamma] \quad (16)$$

which conserve the value of the mapping Hamiltonian. Applying the covariance relation under the diabatic-to-adiabatic transformation (as explicitly discussed in Section 4.1 of ref 17), one obtains the corresponding EOMs in the adiabatic representation

$$\dot{\tilde{\mathbf{x}}}(\mathbf{R}) + i\dot{\tilde{\mathbf{p}}}(\mathbf{R}) = -i\mathbf{V}^{(\text{eff})}(\mathbf{R}, \mathbf{P})(\tilde{\mathbf{x}}(\mathbf{R}) + i\tilde{\mathbf{p}}(\mathbf{R})) \quad (17)$$

$$\dot{\mathbf{R}} = \mathbf{M}^{-1}\mathbf{P} \quad (18)$$

$$\begin{aligned} \dot{\mathbf{P}} &= - \sum_k \nabla_{\mathbf{R}} E_k(\mathbf{R}) \left[\frac{1}{2} ((\tilde{x}^{(k)})^2 + (\tilde{p}^{(k)})^2) - \tilde{\Gamma}_{kk} \right] \\ &- \sum_{k \neq l} [(E_k(\mathbf{R}) - E_l(\mathbf{R})) \mathbf{d}_{lk}(\mathbf{R})] \left[\frac{1}{2} (\tilde{x}^{(k)} \tilde{x}^{(l)} + \tilde{p}^{(k)} \tilde{p}^{(l)}) - \tilde{\Gamma}_{kl} \right] \end{aligned} \quad (19)$$

$$\dot{\tilde{\Gamma}} = i[\tilde{\Gamma}\mathbf{V}^{(\text{eff})}(\mathbf{R}, \mathbf{P}) - \mathbf{V}^{(\text{eff})}(\mathbf{R}, \mathbf{P})\tilde{\Gamma}] \quad (20)$$

In eqs 17–20, $\{\tilde{\mathbf{x}}, \tilde{\mathbf{p}}, \tilde{\Gamma}\} \equiv \{\tilde{\mathbf{x}}(\mathbf{R}), \tilde{\mathbf{p}}(\mathbf{R}), \tilde{\Gamma}(\mathbf{R})\}$ are the mapping phase space variables and commutator matrix for discrete electronic DOFs in the adiabatic representation, and the element of the effective potential matrix, $\mathbf{V}^{(\text{eff})}$, is a function of the nuclear phase space variables

$$\begin{aligned} V_{nk}^{(\text{eff})}(\mathbf{R}, \mathbf{P}) &= E_n(\mathbf{R}) \delta_{nk} - i\dot{\mathbf{R}} \cdot \mathbf{d}_{nk}(\mathbf{R}) \\ &= E_n(\mathbf{R}) \delta_{nk} - i\mathbf{M}^{-1}\mathbf{P} \cdot \mathbf{d}_{nk}(\mathbf{R}) \end{aligned} \quad (21)$$

Equation 19 is produced because the nonadiabatic coupling vector in the adiabatic representation

$$\mathbf{d}_{mn}(\mathbf{R}) = \left\langle \phi_m(\mathbf{R}) \left| \frac{\partial \phi_n(\mathbf{R})}{\partial \mathbf{R}} \right. \right\rangle \quad (22)$$

satisfies $\mathbf{d}_{mn}(\mathbf{R}) = -\mathbf{d}_{nm}(\mathbf{R})$ when the electronic wave function of the basis set is often real for molecular systems. (It is trivial to extend the framework to cases where the electronic wave function of the basis set is complex, e.g., the spin adiabatic state of molecular systems that include spin–orbit coupling terms.) The J -th component of the left-hand side (LHS) of eq 22 is $d_{mn}^{(J)}(\mathbf{R})$. It is straightforward to see that $-i\mathbf{d}^{(J)}(\mathbf{R})$ is a Hermitian matrix of the electronic state DOFs. Vector $-i\mathbf{d}(\mathbf{R})$ indicates a non-abelian gauge field,⁴⁶ which is a generalization of the vector potential of the electromagnetic field.⁴⁷ The EOMs in the adiabatic representation, eqs 17–20, also conserve the mapping Hamiltonian (obtained in the diabatic representation), eq 4, which in the adiabatic representation becomes

$$\begin{aligned} H_C(\tilde{\mathbf{R}}, \tilde{\mathbf{P}}, \tilde{\mathbf{x}}, \tilde{\mathbf{p}}) &\equiv H_C(\mathbf{R}, \mathbf{P}, \tilde{\mathbf{x}}, \tilde{\mathbf{p}}) \\ &= \frac{1}{2}\mathbf{P}(\tilde{\mathbf{P}}, \tilde{\mathbf{x}}, \tilde{\mathbf{p}}, \tilde{\mathbf{R}})^T \mathbf{M}^{-1} \mathbf{P}(\tilde{\mathbf{P}}, \tilde{\mathbf{x}}, \tilde{\mathbf{p}}, \tilde{\mathbf{R}}) \\ &+ \sum_{n=1}^F E_n(\tilde{\mathbf{R}}) \left(\frac{1}{2}((\tilde{x}^{(n)}(\tilde{\mathbf{R}}))^2 + (\tilde{p}^{(n)}(\tilde{\mathbf{R}}))^2) - \tilde{\Gamma}_{nn} \right) \end{aligned} \quad (23)$$

of which the canonical variables on mapping phase space for nuclear DOFs in the adiabatic representation, $\{\tilde{\mathbf{R}}, \tilde{\mathbf{P}}\}$, are

$$\begin{aligned} \tilde{\mathbf{R}} &= \mathbf{R} \\ \tilde{\mathbf{P}} &= \mathbf{P} + i \sum_{m,n} \left[\frac{1}{2}(\tilde{x}^{(n)} + i\tilde{p}^{(n)})(\tilde{x}^{(m)} - i\tilde{p}^{(m)}) - \tilde{\Gamma}_{nm} \right] \mathbf{d}_{mn}(\mathbf{R}) \end{aligned} \quad (24)$$

The mapping diabatic momentum, \mathbf{P} , is intrinsically the kinematic momentum of the adiabatic representation. Owing to the strategy suggested by Cotton et al. for the Meyer–Miller mapping Hamiltonian model,⁴⁸ it is more convenient to employ the EOMs for $\{\mathbf{R}, \mathbf{P}, \tilde{\mathbf{x}}, \tilde{\mathbf{p}}, \tilde{\Gamma}\}$ to avoid the derivative of nonadiabatic coupling terms. The generalized phase space formulation makes it clear that the kinematic nuclear momentum of the adiabatic representation is intrinsically the mapping nuclear momentum, \mathbf{P} , in the diabatic representation.¹⁷ It is then not surprising that the EOMs eqs 17–20 can *not* be generated by the mapping Hamiltonian eq 23, although its value (the mapping energy) is conserved.

As also discussed in Appendix 2 of the Supporting Information of ref 17, the EOMs in the adiabatic representation, eqs 17–20, are valid only when the gauge field tensor

$$\frac{\partial(-i\mathbf{d}^{(I)})}{\partial\tilde{\mathbf{R}}_I} - \frac{\partial(-i\mathbf{d}^{(I)})}{\partial\tilde{\mathbf{R}}_J} + i[-i\mathbf{d}^{(I)}, -i\mathbf{d}^{(J)}]_{\text{ele}} \quad (25)$$

is always zero. This holds only when infinite adiabatic states are considered, or equivalently, when the diabatic representation exists.¹⁷ Since a physical process involves only finite (active) energy, when F electronic states are effectively complete to describe the process, the gauge field tensor, eq 25, is nearly zero and may be neglected with caution.

In addition, as we have first explicitly indicated in the fewest-switches surface hopping (FSSH) applications of ref 17, the kinematic momentum of the adiabatic representation (i.e., the mapping nuclear momentum in the diabatic representation) was also inherently used in SH methods. For example, the “energy” of the hopping trajectory on the PES of the occupied adiabatic state (the j_{occ} -th state), $E_{SH} \equiv \frac{1}{2}\mathbf{P}^T \mathbf{M}^{-1} \mathbf{P} + E_{j_{occ}}(\mathbf{R})$, in most SH methods^{32,33,37,39} intrinsically involves \mathbf{P} , the kinematic momentum of the adiabatic representation, or equivalently the mapping nuclear momentum in the diabatic representation. This is what we have implemented for FSSH in the adiabatic representation in comparison to CPS mapping approaches in refs 16–18.

Ehrenfest-like dynamics governed by eq 16 in the diabatic representation or by eqs 17–20 in the adiabatic representation (inherently generated from the symplectic structure of the diabatic mapping Hamiltonian, eq 4) can be employed for the trajectory with the initial condition eq 27 in the phase space integral expression eq 15 (in either the diabatic or adiabatic representation) for time-dependent properties. This leads to the classical mapping model with commutator variables

(CMMcv), a CPS nonadiabatic dynamics approach that works well for typical condensed phase benchmark models where the states remain coupled all the time but less well for Tully’s gas phase scattering models where asymptotic regions exist.¹⁵ As discussed in ref 17, the EOMs on mapping phase space (of our CPS approaches) are covariant under the transformation of electronic basis sets, e.g., independent of whether the adiabatic or diabatic representation is employed. It is a merit of Ehrenfest-like dynamics. Cotton et al. have already drawn a similar conclusion for the Meyer–Miller mapping Hamiltonian model.⁴⁸

In this Perspective we will focus on the EOMs on quantum phase space in the adiabatic representation. This is due to two major reasons:

- (1) The previous investigation of nuclear quantum statistic mechanical properties by the imaginary time path integral approach for nonadiabatic systems indicates that, compared to exact thermodynamic properties, the adiabatic representation leads to more favorable estimations when the number of path integral beads is one, i.e., in the nuclear classical limit.⁴⁹ The adiabatic representation is then also preferable for further theoretical investigation of the EOMs of the real-time trajectory for nuclear DOFs in the generalized coordinate–momentum phase space formulation.
- (2) It is relatively easy to apply electronic structure methods to obtain the electronically adiabatic basis sets as well as the adiabatic nuclear force on the Born–Oppenheimer PES for most real molecular systems, where the electronically diabatic basis sets are often not rigorously defined.

Initial Condition for Electronic Phase Space Variables in the Adiabatic Representation. As described in ref 15 and its Supporting Information, provided that the j_{occ} -th diabatic electronic state is occupied at the beginning, the initial condition $\tilde{\Gamma}(0)$ for the commutator matrix is

$$\tilde{\Gamma}_{nm}(0) = \left(\frac{1}{2}((\tilde{x}^{(n)}(0))^2 + (\tilde{p}^{(n)}(0))^2) - \delta_{n,j_{occ}} \right) \delta_{nm} \quad (26)$$

Electronic phase space variables $\{\tilde{\mathbf{x}}(0), \tilde{\mathbf{p}}(0), \tilde{\Gamma}(0)\}$ in the adiabatic presentation can then be obtained from $\{\mathbf{x}(0), \mathbf{p}(0), \Gamma(0)\}$ by the diabatic-to-adiabatic transformation before the EOMs in the adiabatic representation are used for propagation of the trajectory.

Alternatively, when the j_{occ} -th adiabatic electronic state is occupied, the initial condition $\tilde{\Gamma}(0)$ for the commutator matrix is

$$\tilde{\Gamma}_{nm}(0) = \left(\frac{1}{2}((\tilde{x}^{(n)}(0))^2 + (\tilde{p}^{(n)}(0))^2) - \delta_{n,j_{occ}} \right) \delta_{nm} \quad (27)$$

In either case, the initial values of electronic phase space variables, $(\tilde{x}^{(n)}(0), \tilde{p}^{(n)}(0))$ in the diabatic representation or $(\tilde{x}^{(n)}(0), \tilde{p}^{(n)}(0))$ in the adiabatic representation, are uniformly sampled from CPS defined by eq 8.

The symplectic integrator of the evolution of electronic phase space variables in the adiabatic representation (eqs 17 and 20) at each nuclear phase point $(\mathbf{R}(t), \mathbf{P}(t))$ reads

$$\begin{aligned} \tilde{\mathbf{g}}(t + \Delta t) &= \tilde{\mathbf{U}}(\mathbf{R}, \mathbf{P}; \Delta t) \tilde{\mathbf{g}}(t) \\ \tilde{\Gamma}(t + \Delta t) &= \tilde{\mathbf{U}}(\mathbf{R}, \mathbf{P}; \Delta t) \tilde{\Gamma}(t) \tilde{\mathbf{U}}^\dagger(\mathbf{R}, \mathbf{P}; \Delta t) \end{aligned} \quad (28)$$

Here, $\tilde{\mathbf{g}}(t) = \tilde{\mathbf{x}}(\mathbf{R}(t); t) + i\tilde{\mathbf{p}}(\mathbf{R}(t); t)$ and $\tilde{\mathbf{U}}(\mathbf{R}(t), \mathbf{P}(t); \Delta t) = \exp[-i\Delta t \mathbf{V}^{(\text{eff})}(\mathbf{R}(t), \mathbf{P}(t))]$ are used. It is heuristic to examine the EOMs for nuclear phase space variables, especially the nuclear force.

Adiabatic and Nonadiabatic Nuclear Force Terms. For simplicity we define

$$\tilde{\rho}_{kl}(\tilde{\mathbf{x}}, \tilde{\mathbf{p}}, \tilde{\Gamma}) = \frac{1}{2}(\tilde{x}^{(k)}\tilde{x}^{(l)} + \tilde{p}^{(k)}\tilde{p}^{(l)}) - \tilde{\Gamma}_{kl} \quad (29)$$

The EOM of eq 19 becomes

$$\dot{\mathbf{P}} = -\sum_k \nabla_{\mathbf{R}} E_k(\mathbf{R})\tilde{\rho}_{kk} - \sum_{k \neq l} [(E_k(\mathbf{R}) - E_l(\mathbf{R}))\mathbf{d}_{lk}(\mathbf{R})]\tilde{\rho}_{kl} \quad (30)$$

It is important to understand the two terms of the Ehrenfest-like force (for updating \mathbf{P}) in the right-hand side (RHS) of eq 30 in the adiabatic representation. The first term is the weighted adiabatic force, i.e., the sum of weighted gradients of all adiabatic PESs. The second term of the RHS of eq 30 is from the contribution related to nonadiabatic couplings between different (adiabatic) electronic states. Such a term is the *intrinsic* nonadiabatic nuclear force that accounts for nonadiabatic transition processes, which should *never* be ignored in the EOMs for nuclear variables in the coupling region. The nonadiabatic nuclear force, the second term of the RHS of eq 30

$$\mathbf{f}_{\text{nonadia.}} = -\sum_{k \neq l} [(E_k(\mathbf{R}) - E_l(\mathbf{R}))\mathbf{d}_{lk}(\mathbf{R})]\tilde{\rho}_{kl} \quad (31)$$

naturally vanishes in the asymptotic region where the nonadiabatic coupling disappears.

On the other hand, the weighted adiabatic force, the first term of the RHS of eq 30, accounts for the unphysical picture of nuclear dynamics even in the asymptotic region. Instead of the average adiabatic force, the adiabatic force term should be from the gradient of the adiabatic PES of a single electronic state. A few nonadiabatic field approaches can be proposed to address the problem of the adiabatic force term, while maintaining eq 31, the nonadiabatic nuclear force term, in eq 19, i.e., in the EOM for updating \mathbf{P} , the kinematic nuclear momentum of the adiabatic representation. That is, gauge field tensor eq 25 in the nonadiabatic field is effectively zero, and the nonadiabatic field involves the original nonadiabatic force term (eq 31) in addition to a single-state adiabatic nuclear force.

Nonadiabatic Field. There exist two simple but reasonable approaches. The first approach is to stochastically choose an ingredient in the sum of the first term in the RHS of eq 30 based on its “weight”. That is, it is more physical to keep a single-state adiabatic force (the gradient of the adiabatic PES), rather than the weighted/average adiabatic force $-\sum_k \nabla_{\mathbf{R}} E_k(\mathbf{R})\tilde{\rho}_{kk}$, for the first term of the RHS of eq 19 of the EOMs. The second approach is to select the dominant ingredient in the sum of the first term in the RHS of eq 30, i.e., the single-state adiabatic nuclear force that takes the largest weight. This ignores the contribution of adiabatic force ingredients with smaller weights. Meanwhile, in either approach, the nonadiabatic nuclear force term eq 31, the second term of the RHS of eq 19, stays the same. As shown in Section S4 of the Supporting Information of this Perspective, the two approaches lead to almost the same results for several benchmark condensed phase model systems.

Because the single-state adiabatic nuclear force component is switched more frequently in the former approach than in the latter one, we choose the latter approach for simplicity. Equation 19 then becomes

$$\dot{\mathbf{P}} = -\sum_k \nabla_{\mathbf{R}} E_k(\mathbf{R}) \left(\prod_{j \neq k} h(\tilde{\rho}_{kk} - \tilde{\rho}_{jj}) \right) - \sum_{k \neq l} [(E_k(\mathbf{R}) - E_l(\mathbf{R}))\mathbf{d}_{lk}(\mathbf{R})]\tilde{\rho}_{kl} \quad (32)$$

Here, $h(y) := \begin{cases} 1 & (y \geq 0) \\ 0 & (y < 0) \end{cases}$ is the Heaviside function. The new

EOMs now include eqs 17, 18, 20, and 32. In addition, the initial value of mapping Hamiltonian eq 23 or mapping energy should also be conserved during the evolution. Because we choose the dominant single-state adiabatic nuclear force in the EOMs for each time step, it suggests that in mapping Hamiltonian eq 23, we should keep the corresponding occupied single-state adiabatic potential. That is, when the j_{occ} -th adiabatic state PES contributes the adiabatic nuclear force, mapping Hamiltonian becomes

$$H_C(\mathbf{R}_0, \mathbf{P}_0, \tilde{\mathbf{x}}_0, \tilde{\mathbf{p}}_0) = H_{\text{NAF}}(\mathbf{R}, \mathbf{P}, \tilde{\mathbf{x}}(\mathbf{R}), \tilde{\mathbf{p}}(\mathbf{R})) \equiv \frac{1}{2}\mathbf{P}^T \mathbf{M}^{-1} \mathbf{P} + E_{j_{\text{occ}}}(\mathbf{R}) \quad (33)$$

Similar to Ehrenfest-like dynamics on mapping phase space, although the mapping Hamiltonian, eq 33, should be conserved during the evaluation, it should *not* be used to yield the EOMs for mapping phase space variables in the adiabatic representation. The kinematic nuclear momentum of the adiabatic representation, \mathbf{P} , is rescaled along the momentum vector (after the update of \mathbf{P} in eq 32) every time step to satisfy the mapping energy conservation.

When the adiabatic electronic state that has the largest “weight” is switched, the kinematic nuclear momentum, \mathbf{P} , should also be rescaled along its original direction such that the mapping energy is conserved. If the dominate weight is switched from the j_{old} -th state component to the j_{new} -th state component, but it is impossible to rescale the momentum to conserve the mapping energy, i.e., $H_C(\mathbf{R}_0, \mathbf{P}_0, \tilde{\mathbf{x}}_0, \tilde{\mathbf{p}}_0) < E_{j_{\text{new}}}(\mathbf{R})$, then the switching of the adiabatic nuclear force component in eq 32 is unphysical. In such a case, the switching is frustrated/prohibited and the single-state adiabatic nuclear force (the first term of the RHS of eq 32) for the evolution of nuclear phase space variables $\{\mathbf{R}, \mathbf{P}\}$ is still from $-\nabla_{\mathbf{R}} E_{j_{\text{old}}}(\mathbf{R})$, the gradient of the previously occupied adiabatic PES even though its “weight” is now not the largest. The integrator of the EOMs of NAF for each time step is described in Section S3 of the Supporting Information.

The EOMs of NAF (e.g., eqs 17, 18, 20, and 32) on quantum phase space are *not* covariant under the transformation of electronic basis sets. NAF should be used in the adiabatic representation. Because the EOMs of NAF are obtained in the generalized quantum coordinate–momentum phase space formulation, we also use eq 15 for the phase space integral expression of time-dependent properties and eq 27 (or eq 26) for the initial condition for electronic mapping variables on CPS. They are the three key elements of NAF, the trajectory-based quantum dynamics method that we propose in this Perspective.

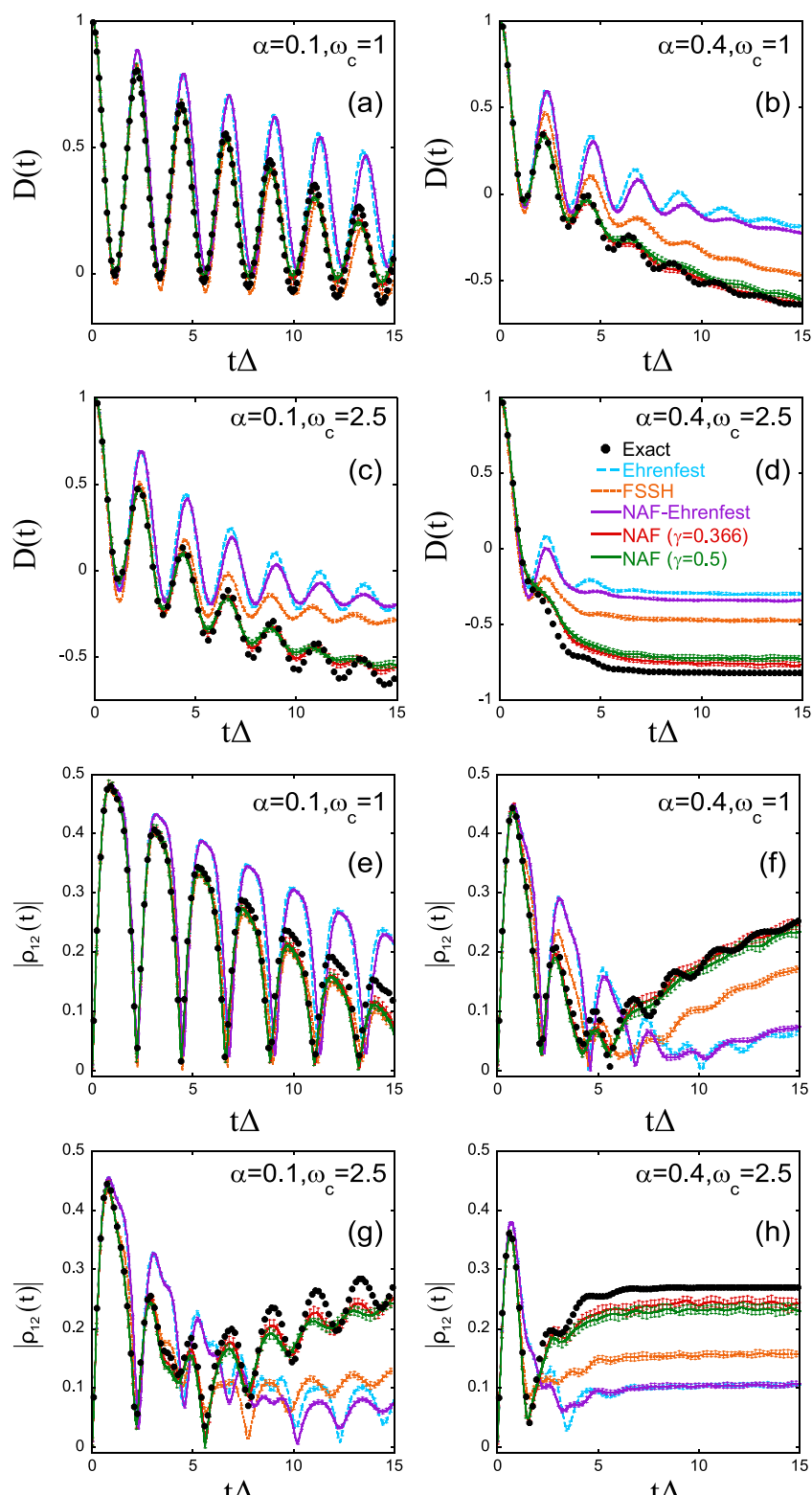


Figure 1. (a–d) Population difference between state 1 and state 2, $D(t)$, as a function of time for spin-boson models with Ohmic spectral density at $\beta = 5$. Panels a–d represent the results of the models with parameters $\{\alpha = 0.1, \omega_c = 1\}$, $\{\alpha = 0.4, \omega_c = 1\}$, $\{\alpha = 0.1, \omega_c = 2.5\}$, and $\{\alpha = 0.4, \omega_c = 2.5\}$, respectively. Black points: Exact results (produced by eHEOM). Cyan long-dashed lines: Ehrenfest dynamics. Orange short-dashed lines: FSSH. Purple, red, and green solid lines: NAF-Ehrenfest, NAF ($\gamma = 0.366$), and NAF ($\gamma = 0.5$), respectively. Panels e–h are the same as panels a–d but for the module of the off-diagonal term $|\rho_{12}(t)|$. Three hundred discrete bath modes are used to obtain converged results. Please see Section S1-A of the Supporting Information.

NAF is exact in the frozen-nuclei limit. When nonadiabatic couplings are constant and nonzero, and only dynamics of the

electronic DOFs are involved, NAF recovers the time-dependent Schrodinger equation. NAF also satisfies the

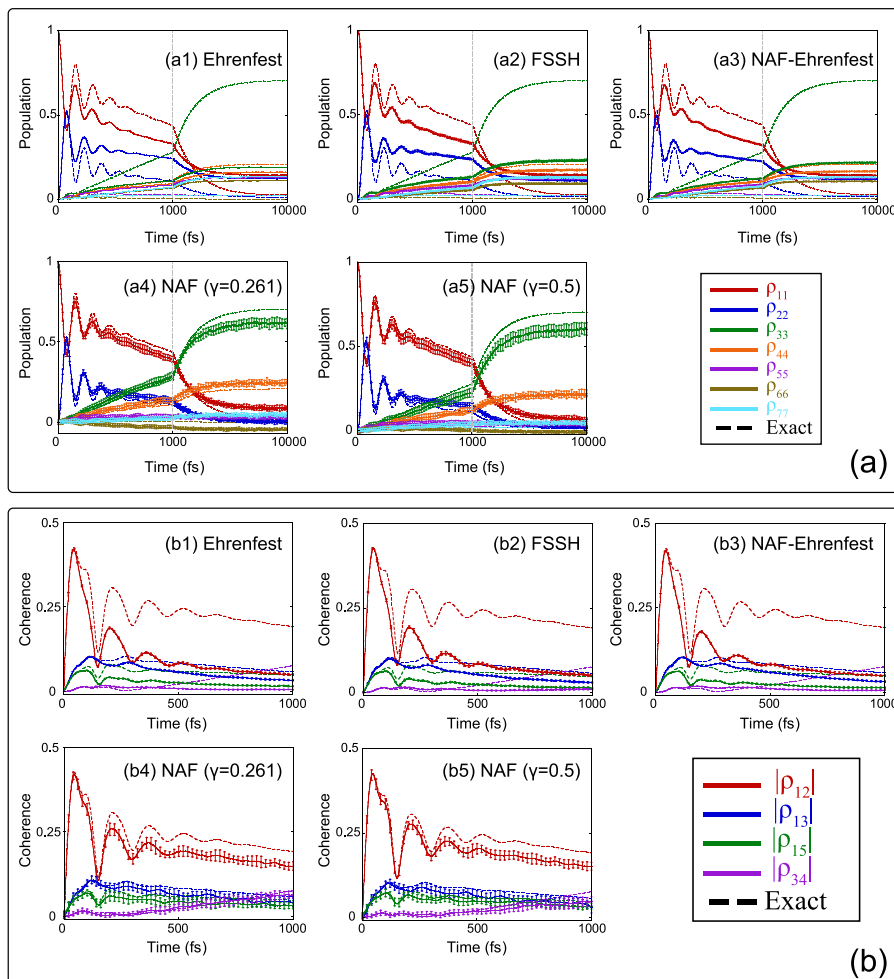


Figure 2. (a) Population dynamics of the FMO model at $T = 77$ K. The initially occupied site is the first site. Panels a1–a5 denote the results of Ehrenfest dynamics, FSSH, NAF-Ehrenfest, NAF ($\gamma = 0.261$) and NAF ($\gamma = 0.5$), respectively, where the red, blue, green, orange, purple, brown, and cyan solid lines represent the population of states 1–7, respectively, and the exact results produced by HEOM are also presented by dashed lines with corresponding colors. Panel b is the same as panel a but for the coherence terms. In panels b1–b5, the red, blue, green, and purple solid lines represent the module of the off-diagonal terms ρ_{12} , ρ_{13} , ρ_{15} , and ρ_{34} , respectively, and the exact results produced by HEOM are also presented by dashed lines with corresponding colors. Fifty discrete bath modes for each site are employed to obtain converged results. Please see Section S1-B of the Supporting Information.

Born–Oppenheimer limit (for the classical nuclear force), where nonadiabatic couplings vanish and a single adiabatic state is occupied. Finally, NAF is exact in the Landau–Zener limit,^{50–53} where the electronic DOFs evolve under the time-dependent Hamiltonian defined by $R(t)$, the coordinate of the nuclear trajectory. We further show the numerical performance of NAF for a few benchmark model systems. Parameter γ of eq 15, the phase space integral expression of time-dependent properties, is chosen in region $[(\sqrt{F+1} - 1)/F, 1/2]$ as suggested in ref 15.

For comparison, we also test the EOMs of NAF with the initial condition and expression for the evaluation of time-dependent (electronic) properties in the conventional mean field approach (NAF-Ehrenfest). This is to demonstrate the importance of the initial condition and that of the integral expression. The conventional Ehrenfest dynamics and FSSH approaches are also tested for comparison. We employ a variant of Tully's FSSH method³⁹ as described in ref 33. This FSSH algorithm is described in Section S7 of the Supporting Information of this Perspective. For fair comparison among trajectory-based nonadiabatic dynamics methods, the initial

condition for nuclear DOFs is sampled from the Wigner distribution on nuclear coordinate–momentum phase space. We consider a few typical benchmark condensed phase and gas phase nonadiabatic models. Numerically exact results of most of these models are available only in the diabatic representation. We perform simulations for all trajectory-based dynamics methods in the adiabatic representation, and the results are then transformed to those in the diabatic representation for the purpose of comparison.

Spin-Boson Models. The spin-boson model depicts a two-state system bilinearly coupled with harmonic bath DOFs of a dissipative environment in the condensed phase.⁵⁴ It also serves as a prototype model for electron/energy transfer/transport in chemical and biological reactions. Numerically exact results of the spin-boson model can be achieved by quasi-adiabatic propagator path integral (QuAPI)^{55–57} and more efficient small matrix PI (SMatPI),^{58,59} hierarchy equations of motion (HEOM),^{60–64} (multilayer) multiconfiguration time-dependent Hartree [(ML-)MCTDH],^{65–67} and time-dependent density matrix renormalization group (TD-DMRG).⁶⁸ The spin-boson model then offers benchmark tests for investigating

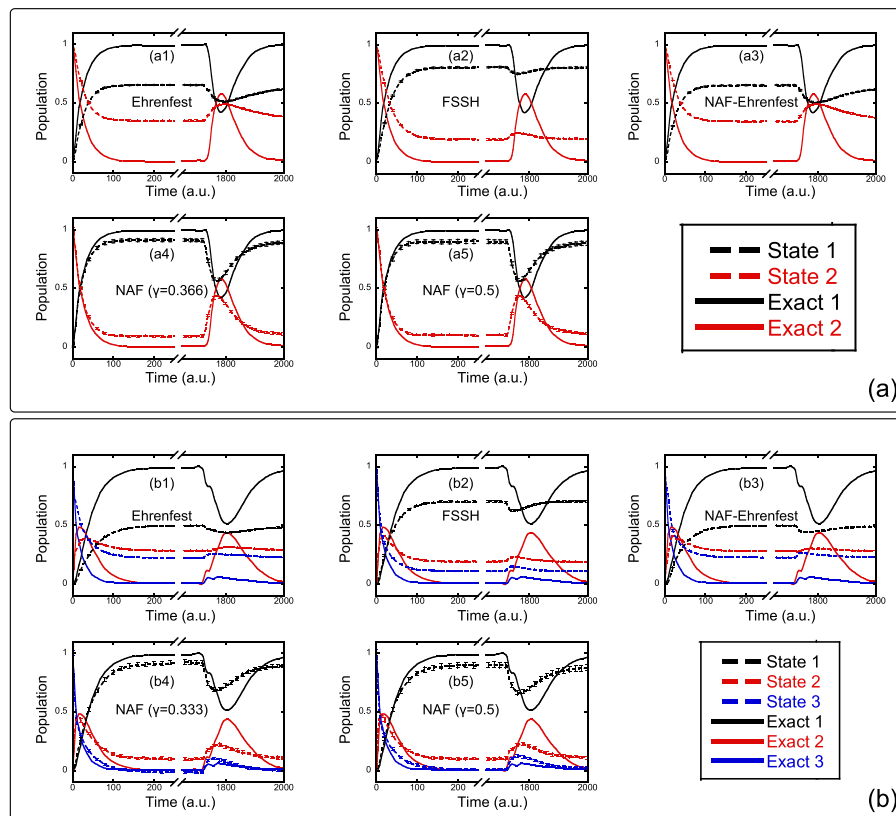


Figure 3. (a) Population dynamics of 2-level atom-in-cavity model. Panels a1–a5 denote the results of Ehrenfest dynamics, FSSH, NAF-Ehrenfest, NAF ($\gamma = 0.366$), and NAF ($\gamma = 0.5$), respectively, where the black and red dashed lines demonstrate the population of state 1 and 2, respectively, and the exact results (from refs 81 and 82) are presented as solid lines with corresponding colors. (b) Population dynamics of the 3-level atom-in-cavity model. Panels b1–b5 denote the results of Ehrenfest dynamics, FSSH, NAF-Ehrenfest, NAF ($\gamma = 0.333$), and NAF ($\gamma = 0.5$), respectively, where the black, red, and blue dashed lines demonstrate the population of states 1–3, respectively, and the exact results (from refs 81 and 82) are presented as solid lines with corresponding colors. Four hundred standing-wave modes for the optical field are used to obtain converged data. Please see Section S1-C of the Supporting Information for more details.

trajectory-based nonadiabatic dynamics methods. We consider the initial condition that the bath modes are at the thermal equilibrium (i.e., the quantum Boltzmann distribution for the pure bath Hamiltonian operator) and the system is in the excited state (the higher energy level). The discretization scheme of refs 69 and 70 is used for obtaining discrete bath modes for the (Ohmic or Debye) spectral density. More numerical details are presented in Section S1-A of the Supporting Information of this Perspective.

Except Ehrenfest dynamics and NAF-Ehrenfest which use the conventional mean field framework, most methods (including FSSH and NAF) perform well for spin-boson models in the high-temperature region, as shown in Figure S5 of the Supporting Information. Here we focus on much more challenging cases in the low-temperature regime. Figure 1 shows the comparison of exact data to numerical results produced by Ehrenfest dynamics, NAF-Ehrenfest, FSSH, and NAF. Neither Ehrenfest dynamics nor FSSH is capable of capturing the correct asymptotic behaviors for population terms (i.e., diagonal elements of the electronic reduced matrix) as well as for “coherence” terms (i.e., off-diagonal elements of the electronic reduced matrix). NAF-Ehrenfest only slightly improves over Ehrenfest dynamics. In contrast, the NAF results show overall good agreement with numerically exact data in the challenging model tests. Although NAF-Ehrenfest and NAF share the same EOMs for real-time dynamics, the two methods employ different formulations of the time-

dependent property as well as different phase space initial conditions. The significant difference between the numerical performance of NAF-Ehrenfest and that of NAF suggests that the formulation of the time-dependent property and that of the phase space initial condition of the trajectory are also important for real-time dynamics methods. NAF with either $\gamma = (\sqrt{F+1} - 1)/F$ or $\gamma = 1/2$ in the integral formulation of time-dependent properties eq 15 leads to nearly the same results. It suggests that NAF is robust when parameter γ lies in the region, $[(\sqrt{F+1} - 1)/F, 1/2]$.

Seven-Site Model for the FMO Monomer. The Fenna–Matthews–Olson (FMO) complex of green sulfur bacteria is a prototype system for studying photosynthetic organisms.^{23,71–77} We consider the site-exciton model of the FMO monomer of ref 74, which describes a seven-site system coupled with a harmonic bath defined by the Debye spectral density. It offers a benchmark model for testing various nonadiabatic dynamics methods. Initially, the bath modes are at thermal equilibrium, and the first site (pigment) is occupied. Numerical details are listed in Section S1-B of the Supporting Information.

We study the evolution of both population and “coherence” terms for the electronic DOFs and plot the results in Figure 2. It is evident that Ehrenfest dynamics performs poorly even for relatively short time and is not capable of even qualitatively capturing the steady-state behavior in the long time limit.

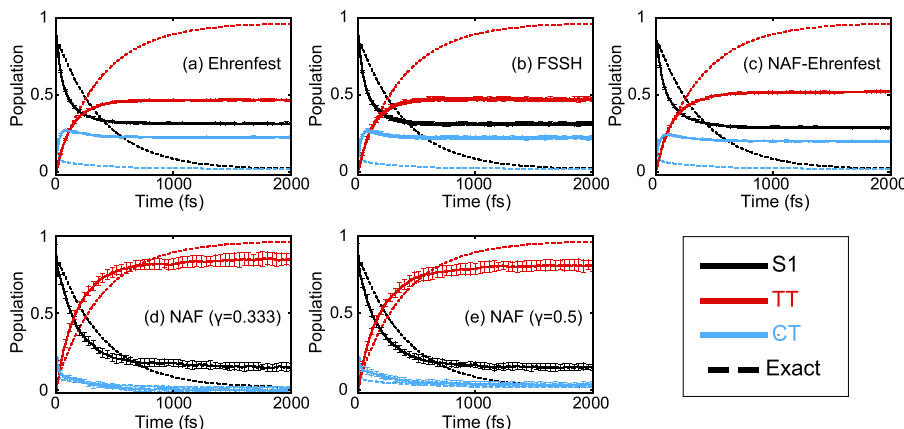


Figure 4. Population dynamics of the SF model at $T = 300$ K. Panels a–e denote the results of Ehrenfest dynamics, FSSH, NAF-Ehrenfest, NAF ($\gamma = 0.333$), and NAF ($\gamma = 0.5$), respectively. In each panel, the black, red, and cyan solid lines represent the population of the S1, TT, and CT states, respectively, and dashed lines with corresponding colors present the exact results produced by HEOM. More numerical details are presented in Section S1-D of the Supporting Information.

NAF-Ehrenfest changes little in comparison with Ehrenfest dynamics. Interestingly, the numerical performance of the FSSH results (produced by the algorithm in ref 33) is also similar to that of the data produced by Ehrenfest dynamics for this test case. In comparison, NAF is competent in quantitatively describing both population and “coherence” terms, even for the asymptotic behavior in the long time limit. The NAF results are relatively insensitive to parameter γ in the region $[(\sqrt{F+1}-1)/F, 1/2]$.

Atom-in-Cavity Models of Cavity Quantum Electrodynamics. It has been reported that a few important phenomena appear in cavity quantum electrodynamics (cQED) especially when matter is strongly coupled to the vacuum field of a confined optical cavity.^{28,78–80} We test two benchmark cQED models that depict a multilevel atom imprisoned in a one-dimensional lossless cavity.^{81–84} The atomic system is coupled to multicavity-modes. The first model involves three atomic levels, and the second one is a reduced two-level model, where only the two lowest levels are considered. At the beginning, the highest atomic level is activated, and all cavity modes are in the vacuum state. The spontaneous emission first happens and releases a photon, which propagates in the cavity and is reflected to meet the atom. The reabsorption and re-emission processes then follow. Numerical details of the two models are described in Section S1-C of the Supporting Information of this Perspective.

As shown in Figure 3, while both Ehrenfest dynamics and FSSH results demonstrate significant deviation even after quite a short time, NAF-Ehrenfest improves little over Ehrenfest dynamics. In contrast, NAF yields much more accurate data for population dynamics of all energy levels and is capable of semiquantitatively describing both the short time behavior and the recoherence around $t = 1800$ au. The performance of NAF is robust when parameter $\gamma \in [(\sqrt{F+1}-1)/F, 1/2]$. It is encouraging that NAF semiquantitatively describes the reabsorption and re-emission processes, while such processes are challenging for both Ehrenfest dynamics and SH methods.

Singlet-Fission Model. Singlet-fission (SF) depicts the conversion of a singlet exciton into two triplet excitons in molecular materials such as solar cells/organic semiconductors.^{24,27,85–87} We use the three-state SF model of ref 86. The system, which includes the singlet (S1) state, charge-transfer

(CT) state, and double triplet (TT) state, is bilinearly coupled to a harmonic bath described by the Debye spectral density. The system–bath coupling of this SF model is relatively strong. It then offers a benchmark model to test nonadiabatic dynamics methods. The initial condition is that the bath modes are at thermal equilibrium and the S1 state is excited. More details are available in Section S1-D of the Supporting Information.

Figure 4 shows that Ehrenfest dynamics and FSSH perform poorly for a relatively long time. While NAF-Ehrenfest is similar to Ehrenfest dynamics for this case, NAF significantly outperforms either Ehrenfest dynamics or FSSH for the asymptotic behavior and leads to much more reasonable long-time results. The numerical results of NAF are nearly the same when parameter $\gamma \in [(\sqrt{F+1}-1)/F, 1/2]$

Gas Phase Models with One Nuclear Degree of Freedom. We have further tested NAF for gas phase models with asymptotic regions. We consider the coupled three-electronic-state photodissociation models of Miller and co-workers.⁸⁸ Each PES is described by a Morse oscillator, and the coupling terms are depicted by Gaussian functions. The initial condition is a nuclear Gaussian wavepacket with electronic state 1 occupied. Numerically exact results for the models can be obtained by the discrete variable representation (DVR) approach.⁸⁹ Please see Section S1-E of the Supporting Information for more numerical details.

It is shown in refs 88 and 90 that when the Ehrenfest trajectory is used in the linearized semiclassical initial value representation (LSC-IVR) of the Stock–Thoss interpretation⁴⁵ of the Meyer–Miller mapping Hamiltonian model,⁴⁴ it fails to even qualitatively yield the nuclear momentum distribution or even electronic population dynamics; the more advanced forward–backward IVR or full SC-IVR^{91–93} is necessary to describe the correct electronic and nuclear dynamics in the asymptotic region. This suggests that the interference between different Ehrenfest trajectories (e.g., in the SC-IVR framework) can lead to the correct nuclear dynamics behavior.^{90,94} While the LSC-IVR of the Stock–Thoss interpretation⁴⁵ of the Meyer–Miller mapping Hamiltonian model⁴⁴ is in principle equivalent to a trajectory-based approach on infinite (Wigner) coordinate–momentum phase space for both continuous nuclear DOFs and discrete electronic DOFs,¹⁷ NAF employs the generalized coordi-

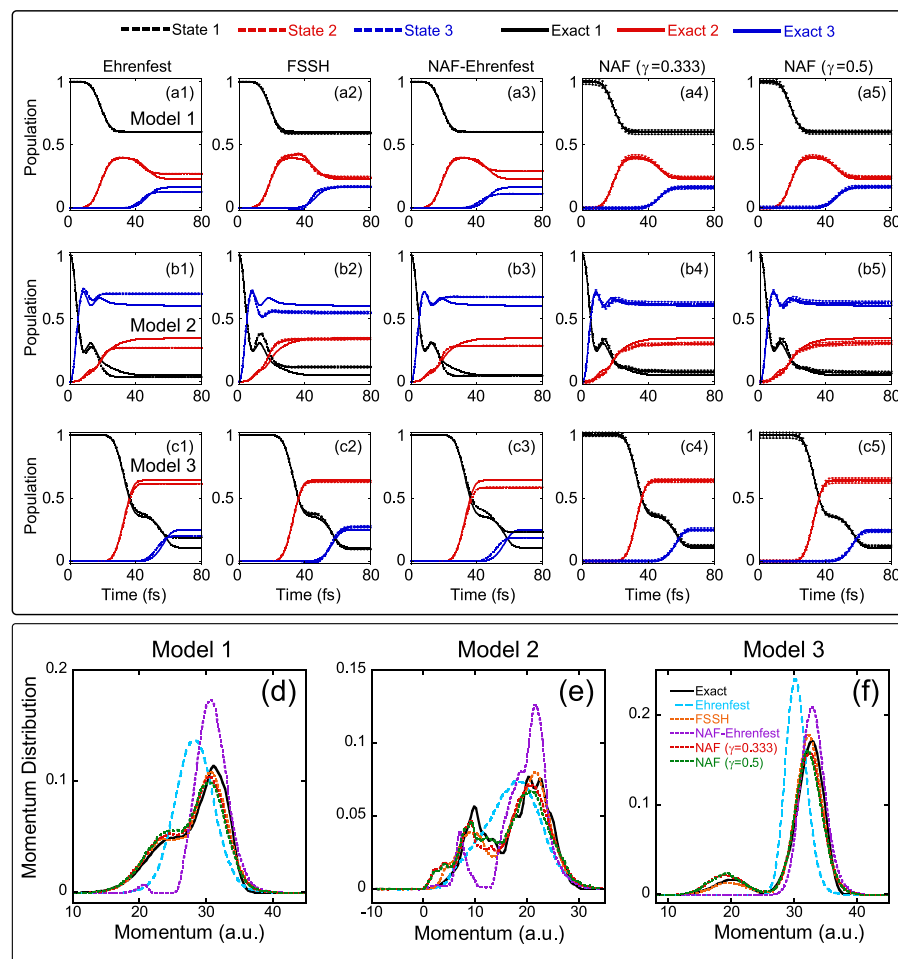


Figure 5. Results of the 3-state photodissociation models. The first three rows [panels a–c] demonstrate the population dynamics of models 1–3, respectively, where the first to fifth columns denote the results of Ehrenfest dynamics, FSSH, NAF-Ehrenfest, NAF ($\gamma = 0.333$), and NAF ($\gamma = 0.5$), respectively. In Panels a–c, the black, red, and blue dashed lines demonstrate the population of states 1–3, respectively, and exact results are presented as solid lines with corresponding colors. Panels d–f demonstrate the nuclear momentum distribution at 200 fs for models 1–3, respectively. Black solid lines: Exact results. Cyan long-dashed lines: Ehrenfest dynamics. Orange short-dashed lines: FSSH. Purple short-dashed lines: NAF-Ehrenfest. Red short-dashed lines: NAF ($\gamma = 0.333$). Green short-dashed lines: NAF ($\gamma = 0.5$). More numerical details are presented in Section S1-E of the Supporting Information.

nate-momentum phase space. It is interesting to test the performance of NAF, which employs only independent trajectories, especially in the asymptotic region.

Figure 5 demonstrates the results for the three-state photodissociation models.⁸⁸ It is indicated that while neither Ehrenfest dynamics nor NAF-Ehrenfest is capable of qualitatively producing the nuclear momentum distribution in the asymptotic region, both FSSH and NAF yield the correct correlation between electronic and nuclear dynamics. Figure 5 also shows that the numerical performance of NAF is insensitive to parameter γ when $\gamma \in [(\sqrt{F+1} - 1)/F, 1/2]$. Similarly, Figures S2 and S4 of the Supporting Information of this Perspective show the data for an asymmetric single avoided crossing (SAC) model. NAF is competent in producing the correct nuclear momentum distribution in the asymptotic region and is capable of performing well for describing electronic dynamics for transmission as well as reflection. Since it is often more expensive to include interference effects among trajectories, it is encouraging to see that NAF performs well even in the asymptotic region without involving phase cancellation among trajectories.

Linear Vibronic Coupling Models for Molecules Involving the Conical Intersection. The linear vibronic coupling model (LVCM) is a simple but effective model that mimics molecular systems where the conical intersection (CI) region plays a critical role in light-driven phenomena. We test the two-electronic-state LVCM with three nuclear modes and that with 24 nuclear modes, which describe the S1/S2 conical intersection of the pyrazine molecule.^{95,96} The initial state is the cross-product of the vibronic ground state and the excited electronic diabatic state (S2). In addition, we study a typical three-electronic-state 2-nuclear-mode LVCM for the Cr(CO)₆ molecule.⁹⁷ The initial condition is the cross-product of the first excited electronically diabatic state and a Gaussian nuclear wave packet. The center of the Gaussian wave packet is located at the minimal point of the ground state of the Cr(CO)₆ molecule that will dissociate a carbonyl group, and the width of each mode is from the corresponding vibrational frequencies.⁹⁷ The details are described in ref 97 and Section S1-F of the Supporting Information of this Perspective. While the diabatic representation is used for the initial condition and evaluation of dynamical properties (as done in MCTDH), the adiabatic representation is employed for real-time dynamics for the fair

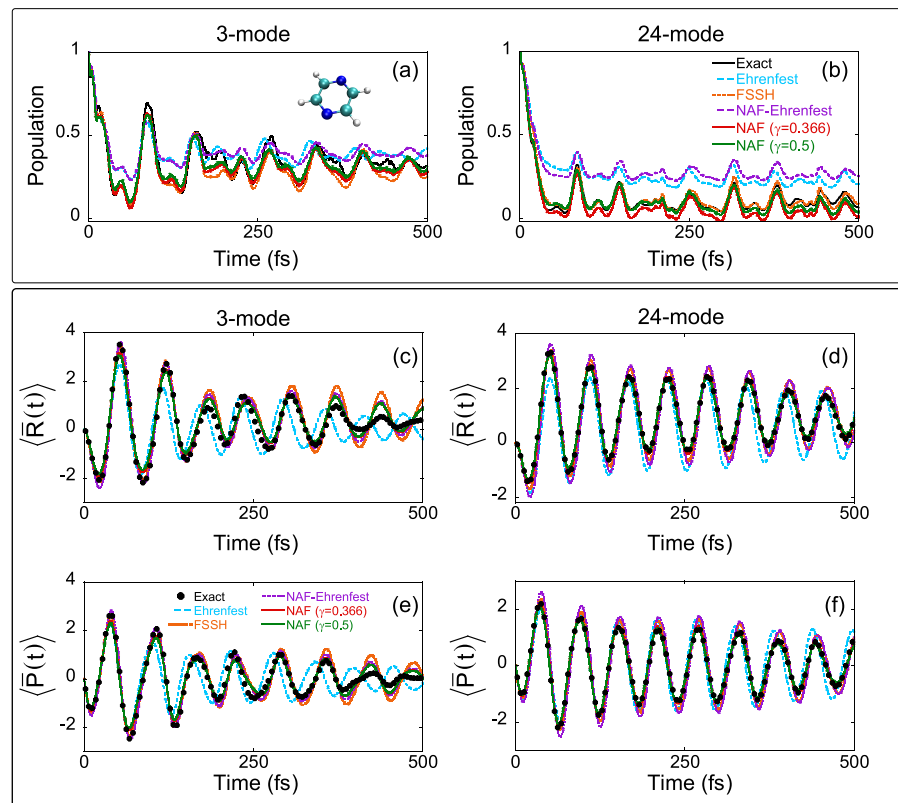


Figure 6. Panels a and b denote population dynamics of the second state of the 2-state LVCM with 3 modes for pyrazine⁹⁵ and that with 24 modes for the same molecule,⁹⁶ respectively. Black solid lines: Exact results produced by MCTDH (ref 98). Cyan long-dashed lines: Ehrenfest dynamics. Orange short-dashed lines: FSSH. Purple long-dashed lines: NAF-Ehrenfest. Red and green solid lines: NAF ($\gamma = 0.366$) and NAF ($\gamma = 0.5$), respectively. Panels c and d demonstrate the average dimensionless coordinate $\langle \bar{R}(t) \rangle$ of the nuclear normal mode v_{6a} of 3-mode and 24-mode LVCMs (for pyrazine), respectively. Black points: Exact results produced by MCTDH.⁹⁸ Cyan long-dashed lines: Ehrenfest. Orange short-dashed lines: FSSH. Purple short-dashed lines: NAF-Ehrenfest. Red and green solid lines: NAF ($\gamma = 0.366$) and NAF ($\gamma = 0.5$), respectively. Panels e and f are the same as panels c and d but for the average dimensionless momentum $\langle \bar{P}(t) \rangle$ of the nuclear normal mode v_{6a} . More numerical details are presented in Section S1-F of the Supporting Information.

comparison among different nonadiabatic dynamics methods. Numerical results are plotted in Figures 6 and 7.

For population dynamics in all of these LVCM cases, FSSH and NAF perform much better than Ehrenfest dynamics and NAF-Ehrenfest. NAF performs slightly better than FSSH for the 2-state 3-mode case of pyrazine. When the 2-state 24-mode case of pyrazine is studied, in comparison to FSSH, NAF yields slightly better nuclear dynamics results but produces a little less accurate electronic population dynamics results. The test results for the 3-state 2-mode LVCM demonstrate that NAF is overall slightly better for population dynamics of the three states. Figures 6 and 7 demonstrate that the overall performance of NAF is comparable to that of FSSH for the LVCM cases for realistic molecular systems. The NAF results are relatively independent of parameter γ in the region, $[(\sqrt{F + 1} - 1)/F, 1/2]$.

In conclusion, the various benchmark model tests of typical gas phase and condensed phase systems (as shown in Figures 1–7) indicate that NAF with CPS is capable of capturing the correct pictures in the coupling region as well as the asymptotic region and shows overall better performance than FSSH as well as Ehrenfest dynamics. Other SH algorithms may lead to different results, but if one honestly treats nuclear DOFs on Wigner phase space to take care of nuclear quantum effects at the beginning, the condensed phase benchmark models (spin-boson, FMO, cQED, and singlet-fission models)

are often challenging for SH methods. In comparison to NAF, the poor performance of NAF-Ehrenfest demonstrates that the integral expression for evaluation of the time-dependent physical property and the initial condition of the trajectory are two important factors for trajectory-based dynamics methods. NAF employs CPS for mapping the discrete electronic-state DOFs, which is rigorous for the initial condition on phase space and more consistent for evaluating dynamic properties. This is missing in the conventional mean field framework as well as in most SH methods. In addition, Section S7 of the Supporting Information demonstrates that fewest switches NAF (FS-NAF), which incorporates the nonadiabatic nuclear force term in the EOMs for nuclear variables of the FSSH algorithm, can systematically improve the numerical performance for condensed phase benchmark models. However, FS-NAF yields less accurate results than NAF. It is expected that the NAF EOMs for nuclear variables are also capable of improving over various other SH methods where the nonadiabatic nuclear force term is never included.

In this Perspective, starting from the generalized exact coordinate–momentum phase space formulation of quantum mechanics, we propose NAF, a conceptually new trajectory-based approach that does not employ the Ehrenfest trajectory or the Born–Oppenheimer trajectory as conventional trajectory-based approaches do. The EOMs of nuclear phase space variables of the NAF trajectory involve the nonadiabatic

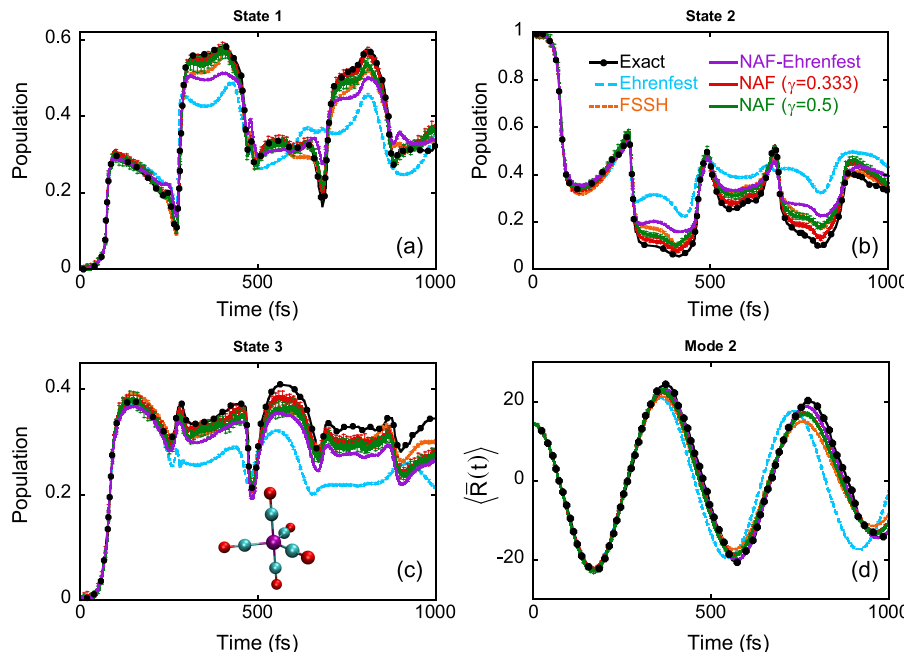


Figure 7. Panels a–c denote population dynamics of states 1–3 of the 2-nuclear-mode LVCM for the $\text{Cr}(\text{CO})_5$ molecule,⁹⁷ respectively. Panel d demonstrates the average dimensionless coordinate $\langle \bar{R}(t) \rangle$ of the second nuclear normal mode. Black solid lines with black points: Exact results produced by MCTDH (obtained from ref 97). Cyan long-dashed lines: Ehrenfest dynamics. Orange short-dashed lines: FSSH. Purple, red, and green solid lines: NAF-Ehrenfest, NAF ($\gamma = 0.333$), and NAF ($\gamma = 0.5$), respectively. More numerical details are presented in Section S1–F of the Supporting Information.

nuclear force term as well as the adiabatic nuclear force term of one single electronically adiabatic state. NAF is exact in the Born–Oppenheimer limit, frozen nuclei limit, and Landau–Zener limit and consistently yields the correlation between electronic and nuclear dynamics in the asymptotic region as well as the state-coupling region. The evaluation of the nuclear force of the NAF trajectory requests no additional effort beyond that in Ehrenfest dynamics as well as FSSH even for *ab initio*-based simulations.^{99–102} NAF involves only independent trajectories on quantum phase space and is practical for real complex/large molecular systems. Despite its various advantages, we expect that NAF of the current version will find it difficult, if not impossible, to describe deep tunneling effects and quantum recurrence/coherence effects, although such effects are often quenched in large molecular systems. For example, it is expected that NAF is not adequate to accurately describe the one-dimensional scattering problem where deep tunneling and quantum resonances dominate.¹⁰³ The time-dependent multiconfiguration approach with NAF trajectories will be a potential candidate to tackle these much more challenging quantum mechanical problems (with more computational effort). In addition to eqs 10 and 15, other exact CPS expressions can also be used for NAF. (For example, NAF with the CPS correlation function of ref 104 is presented in Section S6 of the Supporting Information.) More investigations in the future will shed light on the performance of NAF for more composite systems in chemistry, biology, materials, quantum information and computation, and so forth.

ASSOCIATED CONTENT

Supporting Information

The Supporting Information is available free of charge at <https://pubs.acs.org/doi/10.1021/acs.jpcllett.3c03385>.

Simulation details for models in the main text; additional results for models in the main text; integrator of NAF for a finite time step; comparisons of NAF and NAF(S) results; comparisons of NAF and CMMcv results; comparisons of GDTWA and NAF-GDTWA results; comparisons of NAF, FS-NAF, and FSSH results; details of Ehrenfest dynamics (PDF)

AUTHOR INFORMATION

Corresponding Author

Jian Liu – Beijing National Laboratory for Molecular Sciences, Institute of Theoretical and Computational Chemistry, College of Chemistry and Molecular Engineering, Peking University, Beijing 100871, China; orcid.org/0000-0002-2906-5858; Email: jianliupku@pku.edu.cn

Authors

Baihua Wu – Beijing National Laboratory for Molecular Sciences, Institute of Theoretical and Computational Chemistry, College of Chemistry and Molecular Engineering, Peking University, Beijing 100871, China; orcid.org/0000-0002-1256-6859

Xin He – Beijing National Laboratory for Molecular Sciences, Institute of Theoretical and Computational Chemistry, College of Chemistry and Molecular Engineering, Peking University, Beijing 100871, China; orcid.org/0002-5189-7204

Complete contact information is available at:
<https://pubs.acs.org/10.1021/acs.jpcllett.3c03385>

Notes

The authors declare no competing financial interest.

Biographies

Baihua Wu received his B.S. from the University of Science and Technology Beijing in 2019. He is currently a graduate student in theoretical chemistry at Peking University. His research interests are in phase space mapping approaches of nonadiabatic dynamics.

Xin He received his B.S. from Peking University in 2019. He is currently a graduate student in theoretical chemistry at Peking University. His research interests include phase space mapping theory of nonadiabatic dynamics.

Jian Liu is the Peking University Boya Distinguished Professor. He received his B.S. from the University of Science & Technology of China in 2000 and Ph.D. from the University of Illinois at Urbana-Champaign in 2005. He then did postdoctoral work at the University of California, Berkeley, and was a research associate at Stanford University before he joined Peking University in 2012. His research interests have been focused on the development of phase space formulations of quantum mechanics and trajectory-based methods for studying statistical mechanics and dynamics of complex (large) molecular systems.

ACKNOWLEDGMENTS

We thank Xiangsong Cheng and Youhao Shang for useful discussions. This work was supported by the National Science Fund for Distinguished Young Scholars Grant No. 22225304. We acknowledge the High-performance Computing Platform of Peking University, Beijing PARATERA Tech Co., Ltd., and Guangzhou Supercomputer Center for providing computational resources.

REFERENCES

- (1) Ehrenfest, P.; Ehrenfest, T. Begriffliche Grundlagen Der Statistischen Auffassung in Der Mechanik. In *Encyklopädie Der Mathematischen Wissenschaften*; B. G. Teubner: Liepzig, Germany, 1911; Vol. 4, pp 1–90.
- (2) Nolte, D. D. The Tangled Tale of Phase Space. *Phys. Today* **2010**, *63*, 33–38.
- (3) Goldstein, H.; Poole, C. P.; Safko, J. L. *Classical Mechanics*, 3rd ed.; Addison-Wesley: San Francisco, 2001.
- (4) Arnold, V. I. *Mathematical Methods of Classical Mechanics*; Springer: New York, NY, 2013.
- (5) Weyl, H. Quantum Mechanics and Group Theory. *Z. Phys.* **1927**, *46*, 1–46.
- (6) Wigner, E. On the Quantum Correction for Thermodynamic Equilibrium. *Phys. Rev.* **1932**, *40*, 749–759.
- (7) Groenewold, H. J. On the Principles of Elementary Quantum Mechanics. *Physica* **1946**, *12*, 405–460.
- (8) Moyal, J. E. Quantum Mechanics as a Statistical Theory. *Math. Proc. Cambridge Philos. Soc.* **1949**, *45*, 99–124.
- (9) Lee, H. W. Theory and Application of the Quantum Phase-Space Distribution Functions. *Phys. Rep.* **1995**, *259*, 147–211.
- (10) Cohen, L. Generalized Phase-Space Distribution Functions. *J. Math. Phys.* **1966**, *7*, 781–786.
- (11) Liu, J. A Unified Theoretical Framework for Mapping Models for the Multi-State Hamiltonian. *J. Chem. Phys.* **2016**, *145*, 204105.
- (12) Liu, J. Isomorphism between the Multi-State Hamiltonian and the Second-Quantized Many-Electron Hamiltonian with Only 1-Electron Interactions. *J. Chem. Phys.* **2017**, *146*, 024110.
- (13) He, X.; Liu, J. A New Perspective for Nonadiabatic Dynamics with Phase Space Mapping Models. *J. Chem. Phys.* **2019**, *151*, 024105.
- (14) He, X.; Gong, Z.; Wu, B.; Liu, J. Negative Zero-Point-Energy Parameter in the Meyer-Miller Mapping Model for Nonadiabatic Dynamics. *J. Phys. Chem. Lett.* **2021**, *12*, 2496–2501.
- (15) He, X.; Wu, B.; Gong, Z.; Liu, J. Commutator Matrix in Phase Space Mapping Models for Nonadiabatic Quantum Dynamics. *J. Phys. Chem. A* **2021**, *125*, 6845–6863.
- (16) Liu, J.; He, X.; Wu, B. Unified Formulation of Phase Space Mapping Approaches for Nonadiabatic Quantum Dynamics. *Acc. Chem. Res.* **2021**, *54*, 4215–4228.
- (17) He, X.; Wu, B.; Shang, Y.; Li, B.; Cheng, X.; Liu, J. New Phase Space Formulations and Quantum Dynamics Approaches. *Wiley Interdiscip. Rev. Comput. Mol. Sci.* **2022**, *12*, No. e1619.
- (18) Wu, B.; He, X.; Liu, J. Phase Space Mapping Theory for Nonadiabatic Quantum Molecular Dynamics. In *Volume on Time-Dependent Density Functional Theory: Nonadiabatic Molecular Dynamics*; Zhu, C., Ed.; Jenny Stanford Publishing: New York, 2022.
- (19) Polli, D.; Altoe, P.; Weingart, O.; Spillane, K. M.; Manzoni, C.; Brida, D.; Tomasello, G.; Orlandi, G.; Kukura, P.; Mathies, R. A.; et al. Conical Intersection Dynamics of the Primary Photoisomerization Event in Vision. *Nature* **2010**, *467*, 440–U88.
- (20) Martinez, T. J. Seaming Is Believing. *Nature* **2010**, *467*, 412–413.
- (21) Domcke, W.; Yarkony, D. R.; Köppel, H. *Conical Intersections: Theory, Computation and Experiment*; World Scientific: Singapore, 2011.
- (22) Scholes, G. D.; Fleming, G. R.; Olaya-Castro, A.; van Grondelle, R. Lessons from Nature About Solar Light Harvesting. *Nat. Chem.* **2011**, *3*, 763–774.
- (23) Maiuri, M.; Ostroumov, E. E.; Saer, R. G.; Blankenship, R. E.; Scholes, G. D. Coherent Wavepackets in the Fenna-Matthews-Olson Complex Are Robust to Excitonic-Structure Perturbations Caused by Mutagenesis. *Nat. Chem.* **2018**, *10*, 177–183.
- (24) Smith, M. B.; Michl, J. Singlet Fission. *Chem. Rev.* **2010**, *110*, 6891–6936.
- (25) Scholes, G. D.; Rumbles, G. Excitons in Nanoscale Systems. *Nat. Mater.* **2006**, *5*, 683–696.
- (26) Long, R.; Prezhdo, O. V.; Fang, W.-H. Nonadiabatic Charge Dynamics in Novel Solar Cell Materials. *Wiley Interdiscip. Rev. Comput. Mol. Sci.* **2017**, *7*, No. e1305.
- (27) Wang, Y.-C.; Ke, Y.; Zhao, Y. The Hierarchical and Perturbative Forms of Stochastic Schrödinger Equations and Their Applications to Carrier Dynamics in Organic Materials. *Wiley Interdiscip. Rev. Comput. Mol. Sci.* **2019**, *9*, No. e1375.
- (28) Garcia-Vidal, F. J.; Ciuti, C.; Ebbesen, T. W. Manipulating Matter by Strong Coupling to Vacuum Fields. *Science* **2021**, *373*, No. eabd0336.
- (29) Hammes-Schiffer, S. Theoretical Perspectives on Non-Born-Oppenheimer Effects in Chemistry. *Philos. Trans. Royal Soc. A* **2022**, *380*, 20200377.
- (30) Ehrenfest, P. Bemerkung Über Die Angenäherte Gültigkeit Der Klassischen Mechanik Innerhalb Der Quantenmechanik. *Z. Phys.* **1927**, *45*, 455–457.
- (31) Zhu, C. Y.; Nobusada, K.; Nakamura, H. New Implementation of the Trajectory Surface Hopping Method with Use of the Zhu-Nakamura Theory. *J. Chem. Phys.* **2001**, *115*, 3031–3044.
- (32) Wang, L.; Akimov, A.; Prezhdo, O. V. Recent Progress in Surface Hopping: 2011–2015. *J. Phys. Chem. Lett.* **2016**, *7*, 2100–2112.
- (33) Peng, J.; Xie, Y.; Hu, D.; Du, L.; Lan, Z. Treatment of Nonadiabatic Dynamics by on-the-Fly Trajectory Surface Hopping Dynamics. *Acta Phys.-Chim. Sin.* **2019**, *35*, 28–48.
- (34) Barbatti, M. Nonadiabatic Dynamics with Trajectory Surface Hopping Method. *Wiley Interdiscip. Rev. Comput. Mol. Sci.* **2011**, *1*, 620–633.
- (35) Cui, G.; Thiel, W. Generalized Trajectory Surface-Hopping Method for Internal Conversion and Intersystem Crossing. *J. Chem. Phys.* **2014**, *141*, 124101.
- (36) Mai, S.; Marquetand, P.; González, L. A General Method to Describe Intersystem Crossing Dynamics in Trajectory Surface Hopping. *Int. J. Quantum Chem.* **2015**, *115*, 1215–1231.
- (37) Subotnik, J. E.; Jain, A.; Landry, B.; Petit, A.; Ouyang, W.; Bellonzi, N. Understanding the Surface Hopping View of Electronic Transitions and Decoherence. *Annu. Rev. Phys. Chem.* **2016**, *67*, 387–417.

- (38) Tully, J. C.; Preston, R. K. Trajectory Surface Hopping Approach to Nonadiabatic Molecular Collisions: The Reaction of H^+ with D_2 . *J. Chem. Phys.* **1971**, *55*, 562–572.
- (39) Tully, J. C. Molecular Dynamics with Electronic Transitions. *J. Chem. Phys.* **1990**, *93*, 1061–1071.
- (40) Lang, H. Quantum Dynamics of Chemical Systems with Large Number of Degrees of Freedom: Linearized Phase Space Methods and Quantum Simulations. Ph.D. Dissertation, Ruprecht Karl University of Heidelberg, Heidelberg, Baden-Württemberg, Germany, 2022.
- (41) Nakahara, M. *Geometry, Topology, and Physics*, 2 ed.; Institute of Physics Publishing: Bristol, 2003.
- (42) Atiyah, M. F.; Todd, J. A. On Complex Stiefel Manifolds. *Math. Proc. Cambridge Philos. Soc.* **1960**, *56*, 342–353.
- (43) Shang, Y.; Cheng, X.; Liu, J. (to be submitted).
- (44) Meyer, H.-D.; Miller, W. H. A Classical Analog for Electronic Degrees of Freedom in Nonadiabatic Collision Processes. *J. Chem. Phys.* **1979**, *70*, 3214–3223.
- (45) Stock, G.; Thoss, M. Semiclassical Description of Nonadiabatic Quantum Dynamics. *Phys. Rev. Lett.* **1997**, *78*, 578–581.
- (46) Das, A. *Field Theory*; World Scientific: Singapore, 2019.
- (47) Pacher, T.; Cederbaum, L. S.; Köppel, H. Adiabatic and Quasidiabatic States in a Gauge Theoretical Framework. *Adv. Chem. Phys.* **1993**, *84*, 293–391.
- (48) Cotton, S. J.; Liang, R.; Miller, W. H. On the Adiabatic Representation of Meyer-Miller Electronic-Nuclear Dynamics. *J. Chem. Phys.* **2017**, *147*, 064112.
- (49) Liu, X.; Liu, J. Path Integral Molecular Dynamics for Exact Quantum Statistics of Multi-Electronic-State Systems. *J. Chem. Phys.* **2018**, *148*, 102319.
- (50) Landau, L. D. On the Theory of Transfer of Energy at Collisions II. *Phys. Z. Sowjetunion* **1932**, *2*, 46–51.
- (51) Zener, C. Non-Adiabatic Crossing of Energy Levels. *Proc. R. Soc. London, Ser. A* **1932**, *137*, 696–702.
- (52) Stückelberg, E. C. G. Theory of Inelastic Collisions between Atoms. *Helv. Phys. Acta* **1932**, *5*, 369–423.
- (53) Kyanuma, Y. Nonadiabatic Transitions in Level Crossing with Energy Fluctuation. I. Analytical Investigations. *J. Phys. Soc. Jpn.* **1984**, *53*, 108–117.
- (54) Leggett, A. J.; Chakravarty, S.; Dorsey, A. T.; Fisher, M. P. A.; Garg, A.; Zwerger, W. Dynamics of the Dissipative Two-State System. *Rev. Mod. Phys.* **1987**, *59*, 1–85.
- (55) Makarov, D. E.; Makri, N. Path Integrals for Dissipative Systems by Tensor Multiplication. Condensed Phase Quantum Dynamics for Arbitrarily Long Time. *Chem. Phys. Lett.* **1994**, *221*, 482–491.
- (56) Makri, N.; Makarov, D. E. Tensor Propagator for Iterative Quantum Time Evolution of Reduced Density Matrices. II. Numerical Methodology. *J. Chem. Phys.* **1995**, *102*, 4611–4618.
- (57) Makri, N.; Makarov, D. E. Tensor Propagator for Iterative Quantum Time Evolution of Reduced Density Matrices. I. Theory. *J. Chem. Phys.* **1995**, *102*, 4600–4610.
- (58) Makri, N. Small Matrix Path Integral with Extended Memory. *J. Chem. Theory Comput.* **2021**, *17*, 1–6.
- (59) Makri, N. Small Matrix Disentanglement of the Path Integral: Overcoming the Exponential Tensor Scaling with Memory Length. *J. Chem. Phys.* **2020**, *152*, 041104.
- (60) Tanimura, Y.; Kubo, R. Time Evolution of a Quantum System in Contact with a Nearly Gaussian-Markoffian Noise Bath. *J. Phys. Soc. Jpn.* **1989**, *58*, 101–114.
- (61) Yan, Y.-A.; Yang, F.; Liu, Y.; Shao, J. Hierarchical Approach Based on Stochastic Decoupling to Dissipative Systems. *Chem. Phys. Lett.* **2004**, *395*, 216–221.
- (62) Xu, R.-X.; Cui, P.; Li, X.-Q.; Mo, Y.; Yan, Y. Exact Quantum Master Equation Via the Calculus on Path Integrals. *J. Chem. Phys.* **2005**, *122*, 041103.
- (63) Shao, J. Stochastic Description of Quantum Open Systems: Formal Solution and Strong Dissipation Limit. *Chem. Phys.* **2006**, *322*, 187–192.
- (64) Moix, J. M.; Cao, J. A Hybrid Stochastic Hierarchy Equations of Motion Approach to Treat the Low Temperature Dynamics of Non-Markovian Open Quantum Systems. *J. Chem. Phys.* **2013**, *139*, 134106.
- (65) Meyer, H.-D.; Manthe, U.; Cederbaum, L. S. The Multi-Configurational Time-Dependent Hartree Approach. *Chem. Phys. Lett.* **1990**, *165*, 73–78.
- (66) Thoss, M.; Wang, H.; Miller, W. H. Self-Consistent Hybrid Approach for Complex Systems: Application to the Spin-Boson Model with Debye Spectral Density. *J. Chem. Phys.* **2001**, *115*, 2991–3005.
- (67) Wang, H.; Thoss, M. Multilayer Formulation of the Multiconfiguration Time-Dependent Hartree Theory. *J. Chem. Phys.* **2003**, *119*, 1289–1299.
- (68) Ren, J. J.; Li, W. T.; Jiang, T.; Wang, Y. H.; Shuai, Z. G. Time-Dependent Density Matrix Renormalization Group Method for Quantum Dynamics in Complex Systems. *Wiley Interdiscip. Rev. Comput. Mol. Sci.* **2022**, *12*, No. e1614.
- (69) Makri, N. The Linear Response Approximation and Its Lowest Order Corrections: An Influence Functional Approach. *J. Phys. Chem. B* **1999**, *103*, 2823–2829.
- (70) Wang, H. Iterative Calculation of Energy Eigenstates Employing the Multilayer Multiconfiguration Time-Dependent Hartree Theory. *J. Phys. Chem. A* **2014**, *118*, 9253–9261.
- (71) Fenna, R. E.; Matthews, B. W. Chlorophyll Arrangement in a Bacteriochlorophyll Protein from Chlorobium-Limicola. *Nature* **1975**, *258*, 573–577.
- (72) Engel, G. S.; Calhoun, T. R.; Read, E. L.; Ahn, T. K.; Mancal, T.; Cheng, Y. C.; Blankenship, R. E.; Fleming, G. R. Evidence for Wavelike Energy Transfer through Quantum Coherence in Photosynthetic Systems. *Nature* **2007**, *446*, 782–786.
- (73) Higgins, J. S.; Lloyd, L. T.; Sohal, S. H.; Allodi, M. A.; Otto, J. P.; Saer, R. G.; Wood, R. E.; Massey, S. C.; Ting, P. C.; Blankenship, R. E.; et al. Photosynthesis Tunes Quantum-Mechanical Mixing of Electronic and Vibrational States to Steer Exciton Energy Transfer. *Proc. Natl. Acad. Sci. U. S. A.* **2021**, *118*, No. e2018240118.
- (74) Ishizaki, A.; Fleming, G. R. Theoretical Examination of Quantum Coherence in a Photosynthetic System at Physiological Temperature. *Proc. Natl. Acad. Sci. U. S. A.* **2009**, *106*, 17255–17260.
- (75) Tao, G.; Miller, W. H. Semiclassical Description of Electronic Excitation Population Transfer in a Model Photosynthetic System. *J. Phys. Chem. Lett.* **2010**, *1*, 891–894.
- (76) Miller, W. H. Perspective: Quantum or Classical Coherence? *J. Chem. Phys.* **2012**, *136*, 210901.
- (77) Cao, J. S.; Cogdell, R. J.; Coker, D. F.; Duan, H. G.; Hauer, J.; Kleinkathofer, U.; Jansen, T. L. C.; Mancal, T.; Miller, R. J. D.; Ogilvie, J. P.; et al. Quantum Biology Revisited. *Sci. Adv.* **2020**, *6*, No. eaaz4888.
- (78) Haugland, T. S.; Ronca, E.; Kjønstad, E. F.; Rubio, A.; Koch, H. Coupled Cluster Theory for Molecular Polaritons: Changing Ground and Excited States. *Phys. Rev. X* **2020**, *10*, 041043.
- (79) Toida, H.; Nakajima, T.; Komiyama, S. Vacuum Rabi Splitting in a Semiconductor Circuit QED System. *Phys. Rev. Lett.* **2013**, *110*, 066802.
- (80) Guerin, W.; Santo, T.; Weiss, P.; Cipris, A.; Schachenmayer, J.; Kaiser, R.; Bachelard, R. Collective Multimode Vacuum Rabi Splitting. *Phys. Rev. Lett.* **2019**, *123*, 243401.
- (81) Hoffmann, N. M.; Schäfer, C.; Rubio, A.; Kelly, A.; Appel, H. Capturing Vacuum Fluctuations and Photon Correlations in Cavity Quantum Electrodynamics with Multitrajectory Ehrenfest Dynamics. *Phys. Rev. A* **2019**, *99*, 063819.
- (82) Hoffmann, N. M.; Schäfer, C.; Säkkinen, N.; Rubio, A.; Appel, H.; Kelly, A. Benchmarking Semiclassical and Perturbative Methods for Real-Time Simulations of Cavity-Bound Emission and Interference. *J. Chem. Phys.* **2019**, *151*, 244113.
- (83) Li, T. E.; Chen, H. T.; Nitzan, A.; Subotnik, J. E. Quasiclassical Modeling of Cavity Quantum Electrodynamics. *Phys. Rev. A* **2020**, *101*, 033831.

- (84) Saller, M. A. C.; Kelly, A.; Geva, E. Benchmarking Quasiclassical Mapping Hamiltonian Methods for Simulating Cavity-Modified Molecular Dynamics. *J. Phys. Chem. Lett.* **2021**, *12*, 3163–3170.
- (85) Singh, S.; Jones, W. J.; Siebrand, W.; Stoicoff, B. P.; Schneider, W. G. Laser Generation of Excitons and Fluorescence in Anthracene Crystals. *J. Chem. Phys.* **1965**, *42*, 330–342.
- (86) Chan, W.-L.; Berkelbach, T. C.; Provorse, M. R.; Monahan, N. R.; Tritsch, J. R.; Hybertsen, M. S.; Reichman, D. R.; Gao, J.; Zhu, X.-Y. The Quantum Coherent Mechanism for Singlet Fission: Experiment and Theory. *Acc. Chem. Res.* **2013**, *46*, 1321–1329.
- (87) Casanova, D. Theoretical Modeling of Singlet Fission. *Chem. Rev.* **2018**, *118*, 7164–7207.
- (88) Coronado, E. A.; Xing, J.; Miller, W. H. Ultrafast Non-Adiabatic Dynamics of Systems with Multiple Surface Crossings: A Test of the Meyer-Miller Hamiltonian with Semiclassical Initial Value Representation Methods. *Chem. Phys. Lett.* **2001**, *349*, 521–529.
- (89) Colbert, D. T.; Miller, W. H. A Novel Discrete Variable Representation for Quantum Mechanical Reactive Scattering Via the S-Matrix Kohn Method. *J. Chem. Phys.* **1992**, *96*, 1982–1991.
- (90) Ananth, N.; Venkataraman, C.; Miller, W. H. Semiclassical Description of Electronically Nonadiabatic Dynamics Via the Initial Value Representation. *J. Chem. Phys.* **2007**, *127*, 084114.
- (91) Miller, W. H. Spiers Memorial Lecture - Quantum and Semiclassical Theory of Chemical Reaction Rates. *Faraday Discuss.* **1998**, *110*, 1–21.
- (92) Sun, X.; Miller, W. H. Forward-Backward Initial Value Representation for Semiclassical Time Correlation Functions. *J. Chem. Phys.* **1999**, *110*, 6635–6644.
- (93) Miller, W. H. Quantum Dynamics of Complex Molecular Systems. *Proc. Natl. Acad. Sci. U. S. A.* **2005**, *102*, 6660–6664.
- (94) Miller, W. H. Electronically Nonadiabatic Dynamics Via Semiclassical Initial Value Methods. *J. Phys. Chem. A* **2009**, *113*, 1405–1415.
- (95) Schneider, R.; Domcke, W. S₁-S₂ Conical Intersection and Ultrafast S₂→S₁ Internal Conversion in Pyrazine. *Chem. Phys. Lett.* **1988**, *150*, 235–242.
- (96) Krempel, S.; Winterstetter, M.; Plöhn, H.; Domcke, W. Path-Integral Treatment of Multi-Mode Vibronic Coupling. *J. Chem. Phys.* **1994**, *100*, 926–937.
- (97) Worth, G. A.; Welch, G.; Paterson, M. J. Wavepacket Dynamics Study of Cr(CO)₅ after Formation by Photodissociation: Relaxation through an (E ⊕ A) ⊗ e Jahn-Teller Conical Intersection. *Mol. Phys.* **2006**, *104*, 1095–1105.
- (98) Worth, G. A.; Beck, M. H.; Jackle, A.; Meyer, H.-D. The MCTDH Package, Version 8.2, (2000). H.-D. Meyer, Version 8.3 (2002), Version 8.4 (2007). O. Vendrell and H.-D. Meyer Version 8.5 (2013). Version 8.5 contains the ML-MCTDH algorithm. See <http://mctdh.uni-hd.de>. (accessed 2023-11-01) Used version: 8.5.14.
- (99) Li, X.; Tully, J. C.; Schlegel, H. B.; Frisch, M. J. Ab Initio Ehrenfest Dynamics. *J. Chem. Phys.* **2005**, *123*, 084106.
- (100) Richter, M.; Marquetand, P.; Gonzalez-Vazquez, J.; Sola, I.; Gonzalez, L. SHARC: Ab Initio Molecular Dynamics with Surface Hopping in the Adiabatic Representation Including Arbitrary Couplings. *J. Chem. Theory Comput.* **2011**, *7*, 1253–1258.
- (101) Curchod, B. F. E.; Martínez, T. J. Ab Initio Nonadiabatic Quantum Molecular Dynamics. *Chem. Rev.* **2018**, *118*, 3305–3336.
- (102) Freixas, V. M.; White, A. J.; Nelson, T.; Song, H. J.; Makhov, D. V.; Shalashilin, D.; Fernandez-Alberti, S.; Tretiak, S. Nonadiabatic Excited-State Molecular Dynamics Methodologies: Comparison and Convergence. *J. Phys. Chem. Lett.* **2021**, *12*, 2970–2982.
- (103) He, X.; Wu, B.; Rivlin, T.; Liu, J.; Pollak, E. Transition Path Flight Times and Nonadiabatic Electronic Transitions. *J. Phys. Chem. Lett.* **2022**, *13*, 6966–6974.
- (104) Lang, H.; Vendrell, O.; Hauke, P. Generalized Discrete Truncated Wigner Approximation for Nonadiabatic Quantum-Classical Dynamics. *J. Chem. Phys.* **2021**, *155*, 024111.
- (105) Delos, J. B.; Thorson, W. R.; Knudson, S. K. Semiclassical Theory of Inelastic Collisions. I. Classical Picture and Semiclassical Formulation. *Phys. Rev. A* **1972**, *6*, 709–720.
- (106) Billing, G. D. On the Applicability of the Classical Trajectory Equations in Inelastic Scattering Theory. *Chem. Phys. Lett.* **1975**, *30*, 391–393.
- (107) Miller, W. H.; McCurdy, C. W. Classical Trajectory Model for Electronically Nonadiabatic Collision Phenomena. A Classical Analog for Electronic Degrees of Freedom. *J. Chem. Phys.* **1978**, *69*, 5163–5173.
- (108) Micha, D. A. A Self-Consistent Eikonal Treatment of Electronic Transitions in Molecular Collisions. *J. Chem. Phys.* **1983**, *78*, 7138–7145.
- (109) Shang, Y. On Quantum Phase Space Mapping Theory and Trajectory-Based Dynamics Approaches. B.S. Thesis (Adviser: Jian Liu), Peking University, Beijing, China, 2022.